

This discussion paper is/has been under review for the journal Atmospheric Chemistry and Physics (ACP). Please refer to the corresponding final paper in ACP if available.

Chemical composition and severe ozone loss derived from SCIAMACHY and GOME-2 observations during Arctic winter 2010/2011 in comparisons to Arctic winters in the past

R. Hommel¹, K.-U. Eichmann¹, J. Aschmann¹, K. Bramstedt¹, M. Weber¹,
C. von Savigny^{1,*}, A. Richter¹, A. Rozanov¹, F. Wittrock¹, R. Bauer¹,
F. Khosrawi², and J. P. Burrows¹

¹Institute of Environmental Physics (IUP), University of Bremen, Bremen, Germany

²Department of Meteorology, Stockholm University, Stockholm, Sweden

*now at: Institute of Physics, Ernst-Moritz-Arndt-University of Greifswald, Greifswald, Germany

Received: 1 May 2013 – Accepted: 3 June 2013 – Published: 20 June 2013

Correspondence to: R. Hommel (rene.hommel@iup.physik.uni-bremen.de)

Published by Copernicus Publications on behalf of the European Geosciences Union.

Title Page

Abstract

Introduction

Conclusions

References

Tables

Figures

◀

▶

◀

▶

Back

Close

Full Screen / Esc

Printer-friendly Version

Interactive Discussion



Abstract

Record breaking losses of ozone (O_3) in the Arctic stratosphere have been reported in winter and spring 2011. Trace gas amounts and polar stratospheric cloud (PSC) distributions retrieved using differential optical absorption spectroscopy (DOAS) and scattering theory applied to the measurements of radiance and irradiance by satellite-born and ground-based instrumentation, document the unusual behaviour. A chemical transport model has been used to relate and compare Arctic winter-spring conditions in 2011 with those in previous years. We examine in detail the composition and transformations occurring in the Arctic polar vortex using total column and vertical profile data products for O_3 , bromine oxide (BrO), nitrogen dioxide (NO_2), chlorine dioxide (ClO), and PSCs retrieved from measurements made by the instrument SCIAMACHY on-board the ESA satellite Envisat, as well as the total column ozone amount, retrieved from the measurements of GOME-2 on the EUMETSAT operational meteorological polar orbiter Metop-A. In the late winter and spring 2010/2011 the chemical loss of O_3 in the polar vortex is consistent with and confirms findings reported elsewhere. More than 70 % of O_3 was depleted between the 425 K and 525 K isentropic surfaces, i.e. in the altitude range ~ 16 – 20 km. In contrast, during the same period in the previous winter only slightly more than 20 % depletion occurred below 20 km, whereas 40 % of the O_3 was removed above the 575 K isentrope (~ 23 km). This loss above the 575 K isentrope is explained by the catalytic destruction by the NO_x descending from the mesosphere. At lower altitudes O_3 loss results from processing by halogen driven O_3 catalytic removal cycles, activated by the large volume of PSC generated throughout this winter and spring. The mid-winter 2011 conditions, prior to the catalytic cycles being fully effective, are also investigated. Surprisingly, a significant loss of O_3 with 60 % is observed in mid-January 2011 below 500 K (~ 19 km), which was then sustained for approximately a week. This “mini-hole” event had an exceptionally large spatial extent. Such meteorologically driven changes in polar stratospheric O_3 are expected to increase in frequency as anthropogenically induced climate change evolves.

The Arctic low ozone period 2011

R. Hommel et al.

Title Page

Abstract

Introduction

Conclusions

References

Tables

Figures

◀

▶

◀

▶

Back

Close

Full Screen / Esc

Printer-friendly Version

Interactive Discussion



1 Introduction

Predicting the future levels of ozone (O_3) above the Arctic and its loss during winter-spring is intrinsically challenging. The history of the observations of stratospheric ozone at high latitudes has repeatedly resulted in unexpected behaviour attributable to our limited knowledge of the dynamics and chemistry. Accurate scientific assessments of the evolution of polar ozone in a changing climate are required by the parties to the United Nation's Vienna Convention on Ozone Depleting Substances (ODS) and its Montreal Protocol/amendments.

In the Northern Hemisphere in contrast to the Southern Hemisphere, the polar vortex is much less stable and a large inter-annual variability of stratospheric ozone at mid-and high-latitudes occurs. This variability is closely tied to year-to-year changes in the activity of planetary waves (Fusco and Salby, 1999; Weber et al., 2011), modulating the intensity, temporal evolution and stability of the Arctic polar vortex (see for example Hartmann et al., 2000; Dhomse et al., 2006; Mitchell et al., 2011, and references therein). By determining the vortex temperature, this in turn modulates the effectiveness of the catalytic cycles removing stratospheric O_3 in late winter and spring after polar sunrise via the formation of polar stratospheric clouds (PSC). As a result heterogeneous reactions and equilibria, which take place on aerosol and PSC, convert the relatively photo-stable species such as hydrogen chloride (HCl), chlorine nitrate ($ClONO_2$), bromine nitrate ($BrONO_2$) and hypobromous acid (HOBr) into the photo-labile species molecular chlorine (Cl_2), bromine chloride (BrCl), bromine (Br_2) and related halogen temporary reservoirs. The rate of removal of ozone is thus strongly dependent on particular dynamical conditions in a given winter and spring (WMO, 2010, and references therein). In winter-spring 2011, anomalously large ozone losses in the Arctic stratospheric polar vortex have been reported (e.g. Hurwitz et al., 2011; Manney et al., 2011; Sinnhuber et al., 2011). In March 2010, however, when also the Arctic stratosphere was extensively denitrified and large chlorine activation was observed

ACPD

13, 16597–16660, 2013

The Arctic low ozone period 2011

R. Hommel et al.

Title Page

Abstract

Introduction

Conclusions

References

Tables

Figures

◀

▶

◀

▶

Back

Close

Full Screen / Esc

Printer-friendly Version

Interactive Discussion



(Manney et al., 2011; Khosrawi et al., 2011), polar ozone was unusually high (Steinbrecht et al., 2011).

In spite of the first indications of stratospheric ozone recovering, as a result of the measures enacted by the Montreal Protocol (see WMO, 2010, and references therein) and inferred from the studies of Mäder et al. (2010) and Salby et al. (2011), an ongoing potential for further, yet unexpected, dramatical polar ozone losses exists (e.g. Rex et al., 2004). It is therefore of value to examine the causes of Arctic variability and their impact on polar ozone and its depletion, in order to improve our understanding of the chemical and dynamical control of stratospheric ozone in a changing climate.

In this paper, we investigate the chemical composition of the Arctic vortex during winter–spring 2011, where ozone loss was one of the largest yet observed, and compare it with observations from the preceding winter–spring in 2010, when polar ozone levels were unusually large. Data products from the nadir, limb and occultation measurements of SCIAMACHY for O₃, BrO, NO₂, OCIO and PSCs have been used to determine the compositional state of the Arctic vortex. To put them into the context of the documented inter-annual variability of Arctic ozone, the total column amount of O₃ is retrieved from GOME/SCIAMACHY/GOME-2 nadir measurements for the winters from 1995/1996 to 2011/2012. In addition, we show ground-based DOAS measurements of OCIO and NO₂ over Ny-Ålesund (79° N, 12° E), providing additional information to probe our understanding of the vortex behaviour. Extending the work of Sonkaew et al. (2013), the vertical profile of chemical ozone loss in the Arctic lower stratosphere has been determined for the 2010 and 2011 polar vortices, using the vortex-average method. This method accounts explicitly for the diabatic changes in ozone (Eichmann et al., 2002). By comparison of novel time-slice simulations, conducted with a three-dimensional chemistry transport model (CTM) driven by ECMWF ERA-Interim meteorology, with observations, our understanding and ability to simulate the behaviour of chemistry and dynamics in the years 2010 and 2011 is tested.

The methods and data sources, used to investigate the state of ozone in the Arctic vortex, are described in Sect. 2. This is then followed in Sect. 3 by a more detailed

The Arctic low ozone period 2011

R. Hommel et al.

Title Page

Abstract

Introduction

Conclusions

References

Tables

Figures

◀

▶

◀

▶

Back

Close

Full Screen / Esc

Printer-friendly Version

Interactive Discussion



description of the conditions during winter–spring 2010 and 2011. The origins of an episode of extremely low ozone in mid-winter 2011, previously unreported, which occurred prior to the large chemical destruction of ozone later in spring, is also identified and investigated. Section 4 summarizes our results and interpretation of these two unique winters.

2 Methods

The research, reported in this manuscript, uses the data products retrieved from the Scanning Imaging Absorption SpectroMeter for Atmospheric CHartography (SCIAMACHY) onboard ESA's Envisat satellite (Burrows et al., 1995; Bovensmann et al., 1999) and from the Global Ozone Monitoring Experiment (GOME) instrument onboard ESA's second European Remote Sensing satellite (ERS-2; Burrows et al., 1999) and its operational successor GOME-2 onboard EUMETSAT's Meteorological Operational satellite (MetOp-A). SCIAMACHY was proposed in July 1988 for launch on the ESA Polar Orbiting Earth Mission, POEM-1. This mission was subsequently renamed Envisat and launched on the 28 February 2002 into a polar sun-synchronous orbit similar to ERS-2 at an altitude of about 800 km. SCIAMACHY makes measurements of the back-scattered solar radiation upwelling from the top of the atmosphere for the majority of its orbit, alternately in limb and nadir viewing. During orbital sunrise at mid and high northern latitudes solar occultation measurements are performed, and lunar occultation measurements are made on the nightside of the Earth in the Southern Hemisphere. Solar occultation is undertaken once per orbit whereas the moon is only in view about 6 days a month. Global coverage of the sunlit part of the Earth is achieved at the equator in six days in nadir and limb viewing. Contact with Envisat was unexpectedly and suddenly lost on the 8 April 2012.

For almost a decade SCIAMACHY provided a unique record of the upwelling radiation at the top of the atmosphere in its different viewing geometries simultaneously and contiguously in 6 channels from 214 to 1750 nm and two channels mea-

The Arctic low ozone period 2011

R. Hommel et al.

Title Page

Abstract

Introduction

Conclusions

References

Tables

Figures

◀

▶

◀

▶

Back

Close

Full Screen / Esc

Printer-friendly Version

Interactive Discussion



The Arctic low ozone period 2011

R. Hommel et al.

[Title Page](#)[Abstract](#)[Introduction](#)[Conclusions](#)[References](#)[Tables](#)[Figures](#)[◀](#)[▶](#)[◀](#)[▶](#)[Back](#)[Close](#)[Full Screen / Esc](#)[Printer-friendly Version](#)[Interactive Discussion](#)

suring from 1940 to 2040 nm and 2265 to 2380 nm, respectively. Additionally, polarisation measurements are performed using 7 broad-band polarisation measurement devices (PMDs). Its limb and occultation measurements yield profiles of atmospheric constituents (gases, aerosol and cloud) from the troposphere to the thermosphere. The solar occultation measurements are restricted to the latitudes range from 49 to 69° N. Limb measurements provide global coverage.

The smaller instrument GOME resulted from the descopeing of the SCIA-mini, which was proposed to ESA in response to its call for atmospheric constituent monitoring instrumentation in December 1988. GOME was launched aboard ERS-2 on the 20th April 1995 into a sun-synchronous orbit having an equator crossing time of 10.30 a.m. during the descending part of the orbit. It made global measurements in nadir viewing geometry of the upwelling electromagnetic radiation between 233 and 793 nm from July 1995 to June 2003, when ERS-2 lost its tape recorder. Using its 960 km swath, global coverage at the equator is achieved in three days. After June 2003, 30–40 % of its measurements were downlinked in direct broadcast mode until ESA began decommissioning ERS-2 in July 2011.

The first GOME-2 was launched aboard Metop-A in October 2006 into a sun-synchronous orbit having an descending leg equator crossing time of 9.30 a.m. Routine operations began in March 2007. GOME-2 has a superior spatial resolution to that of GOME, similar to that in nadir of SCIAMACHY. Metop-B with a second GOME-2 has been launched in September 2012. For additional information about the instruments and general measurement techniques we refer readers to the following publications: Burrows et al. (1995) and Bovensmann et al. (1999) for SCIAMACHY; Burrows et al. (1999) and Callies et al. (2000) for GOME and GOME-2, respectively.

2.1 SCIAMACHY limb trace gas profiles

Vertical profiles of atmospheric species are retrieved from limb-scatter measurements performed by the SCIAMACHY instrument on Envisat (Bovensmann et al., 1999). The level 2 data products retrievals used in this investigation (version 2.5) have been devel-

oped and processed at the Institute of the Environmental Physics (IUP) of the University of Bremen (IUP Bremen retrieval) using the level 1 (version 7.03/04) data products provided by ESA. For this study several spectral windows in the UV, visible, or near-infrared spectral ranges have been used.

5 The vertical ozone profile retrieval uses an optimal estimation approach employing the radiance profiles measured at selected wavelengths in the UV Hartley and Huggins bands of O₃ (267–305 nm; Rohen et al., 2008) and the visible O₃ Chappuis band (see Sonkaew et al., 2009). The NO₂ and BrO vertical profiles are retrieved using their fingerprint differential structure of the trace gas absorption bands in the spectral ranges
10 420–470 nm and 338–356.2 nm, respectively.

All these retrievals use an upper atmosphere reference tangent height to normalise the limb radiance at a given tangent height in order to reduce the influence of the solar Fraunhofer lines, any errors in instrument radiometric calibration and radiation scattered in the lower troposphere or reflected from the underlying surface. The position of
15 the reference tangent heights is optimised individually for each species and in the case of ozone with respect to the different spectral intervals used. Both O₃ and BrO retrievals use variants on the optimal estimation type technique (Rodgers, 2000) having an additional smoothing constraint (first order Tikhonov term), while the NO₂ retrieval employs the information operator approach (see Kozlov, 1983; Hoogen et al., 1999; Doicu et al.,
20 2007, and references therein). The pressure and temperature information used in the forward radiative transfer model is provided by the operational analysis model of the European Centre for Medium-Range Weather Forecasts (ECMWF). More detailed explanations of the retrieval algorithms and validation results for different species are reported elsewhere: e.g. for the NO₂ retrieval algorithm in Rozanov et al. (2005); for
25 the O₃ algorithm in Sonkaew et al. (2009); O₃ profile validation results are presented in Mieruch et al. (2012); BrO profile validation is reported by Rozanov et al. (2011a,b); for NO₂ profile validation see Bauer et al. (2012).

The Arctic low ozone period 2011

R. Hommel et al.

[Title Page](#)[Abstract](#)[Introduction](#)[Conclusions](#)[References](#)[Tables](#)[Figures](#)[I◀](#)[▶I](#)[◀](#)[▶](#)[Back](#)[Close](#)[Full Screen / Esc](#)[Printer-friendly Version](#)[Interactive Discussion](#)

2.2 SCIAMACHY solar occultation

SCIAMACHY performs a solar occultation measurement once per orbit. The sun-synchronous polar orbit of Envisat provides seasonally dependent occultations at mid-latitudes. These occur between 49° N and 69° N in the Northern Hemisphere. Vertical profiles of O₃, NO₂, and BrO are retrieved by applying an optimal estimation approach including a smoothing constraint, similar to that used for O₃ and BrO profiles retrieved from the limb measurements. The knowledge of the tangent height for the solar occultation measurements has been optimised using the scans over the solar disk (Bramstedt et al., 2012). In this case O₃ is retrieved from the Chappuis bands between 524.3–590.7 nm. The O₃ profile is then used in the retrieval of NO₂ from the spectral window 424.1–453.3 nm. Previous versions of these products are described in Meyer et al. (2005) and Bramstedt et al. (2007). The vertical profile of BrO is retrieved from the radiance and irradiance measurements in the spectral window 338.0–356.2 nm (using the knowledge of the previously retrieved O₃ and NO₂ profiles). It is for the first time evaluated in this paper, and in this sense a preliminary product. Pressure and temperature information at a given tangent height is based on the ECMWF data also used in the limb retrievals. The solar occultation retrievals are produced using retrieval algorithms developed at IUP Bremen.

2.3 SCIAMACHY OCIO and NO₂ from nadir measurements

SCIAMACHY nadir observations have been analysed for OCIO and NO₂ slant columns retrieved by the Differential Optical Absorption Spectroscopy (DOAS; see Platt, 1994) applied to the measurements of the upwelling radiation from space (see Burrows et al., 2011, and references therein). The analysis performed here closely follows the approach described in Richter et al. (2005) applied to GOME data.

The OCIO molecule, which undergoes rapid photolysis during daytime, achieves its largest concentrations at night and thus is best measured during twilight in nadir sounding. In addition the OCIO amount changes rapidly along the path of electromagnetic

[Title Page](#)[Abstract](#)[Introduction](#)[Conclusions](#)[References](#)[Tables](#)[Figures](#)[◀](#)[▶](#)[◀](#)[▶](#)[Back](#)[Close](#)[Full Screen / Esc](#)[Printer-friendly Version](#)[Interactive Discussion](#)

The Arctic low ozone period 2011

R. Hommel et al.

Title Page

Abstract

Introduction

Conclusions

References

Tables

Figures

◀

▶

◀

▶

Back

Close

Full Screen / Esc

Printer-friendly Version

Interactive Discussion



radiation through the atmosphere and as a function of the solar zenith angle (SZA). These changes can be accounted for by simulation using radiative transfer models (Hendrick et al., 2006; Oetjen et al., 2011, and references therein). However, for the assessment of change, an optimal approach to evaluate changes in OCIO measurements is to compare the data at a solar zenith angle of 90° . This avoids any error in the conversion of slant to vertical columns (Wagner et al., 2002; Richter et al., 2005) and the relative changes between years. For a quantitative comparison with models, the radiative transfer effects need to be accounted for.

At large SZA, the intensity of electromagnetic radiation leaving the top of the atmosphere is small and individual measurements of OCIO retrieved from SCIAMACHY have a relatively low signal to noise and thus large retrieval errors. By averaging over the measurements made at SZAs between 89° and 91° the error and resultant scatter is reduced. This approach has been validated by comparison with ground-based zenith-sky observations where very good agreement was obtained (Oetjen et al., 2011).

NO_2 is also photolysed by ultraviolet radiation but the changes along the path of ultraviolet radiation are smaller than those for OCIO and vertical columns can be determined using an appropriate air mass factors (AMF). However, to be consistent with the OCIO observations, NO_2 columns are also analysed around SZA of 90° . This approach has the additional advantage of a much reduced sensitivity to the lower atmosphere, minimising any potential impact of tropospheric pollution in the Arctic.

2.4 SCIAMACHY PSC detection description

SCIAMACHY provides profile measurements of limb-scattered solar radiation. From the profiles at 750 and 1090 nm we construct a colour index, which is used in combination with a defined threshold to detect PSC. More detailed information on the PSC detection method can be found in von Savigny et al. (2005a). As shown in von Savigny et al. (2005b) the retrievals are robust. For almost all of the detections of PSC the ECMWF temperature at the location and altitude of the detected PSC is consistent with

the known PSC temperature formation threshold of about 195–198 K. The current PSC detection scheme does not allow to distinguish between different PSC types.

In von Savigny et al. (2005a) only PSC observations in the Southern Hemisphere were analysed, while in this study we show results obtained from SCIAMACHY measurements in the Northern Hemisphere for the first time. In contrast to the southern hemispheric observations with scattering angles of up to 160°, the northern hemispheric SCIAMACHY limb-scatter observations – particularly at high latitudes – are associated with relatively small scattering angles as low as about 25°. This difference in scattering angles required a minor optimisation of the PSC detection threshold applied to the vertical gradients of the colour-index ratio. For the analyses presented here a threshold value of $\theta = 1.45$ is used. More detailed information on the PSC detection method can be found in von Savigny et al. (2005a).

2.5 Ground based measurements

Ground-based zenith sky observations made at Ny-Ålesund (79° N, 12° E) have been used to retrieve OCIO and NO₂ slant columns using the Differential Optical Absorption Spectroscopy (DOAS; Platt, 1994) method. The spectral window and related settings are similar to those used with SCIAMACHY radiances for the retrieval of trace gas slant columns. Here, as references spectrum, a measurement at a small solar zenith angle is used: the SZA being typically about 80°. For more details see Oetjen et al. (2011).

2.6 Long-term total column ozone data set

A consistent, consolidated and merged O₃ total column, retrieved from the nadir measurements made by GOME, SCIAMACHY (Bracher et al., 2005) and GOME-2 (Coldewey-Egbers et al., 2005; Weber et al., 2005), called in short the GSG data set, has been compiled at IUP (Weber et al., 2007). In the GSG data set the SCIAMACHY (2002–2012) and the well validated GOME data record (1995–2011) have been used to normalize the data sets by a mean scaling factor (GOME2 and SCIAMACHY) and

The Arctic low ozone period 2011

R. Hommel et al.

Title Page

Abstract

Introduction

Conclusions

References

Tables

Figures

◀

▶

◀

▶

Back

Close

Full Screen / Esc

Printer-friendly Version

Interactive Discussion



trend (SCIAMACHY only) in the monthly mean zonal mean ratios. Using the selection criterion of having maximum global sampling, the GSG data set is then composed of GOME from 1995 to June 2003, SCIAMACHY from 2003 to 2006 and GOME-2 after 2006. This data set has already been used in other related studies (Kieseewetter et al., 2010a,b). Data are available from <http://www.iup.uni-bremen.de/gome/wfdoas>. Another long-term data set is the merged SBUV/TOMS/OMI O₃ data set (Mod V8; http://acdb-ext.gsfc.nasa.gov/Data_services/merged) that extends from 1978 to present (Stolarski and Frith, 2006), which agrees to within 2% with the GSG data set when comparing monthly mean zonal means.

2.7 Chemical ozone loss calculation

The chemical ozone loss has been calculated using ozone profiles retrieved in the polar vortex. This approach has been explained in more detail by Eichmann et al. (2002). The method has been adapted to SCIAMACHY ozone limb profiles using UKMO meteorological data for the determination of the vortex edge and the calculation of diabatic descent rates (Sonkaew et al., 2013). Retrieved SCIAMACHY ozone number density profiles were converted to volume mixing ratios and interpolated to isentropic levels between 425 K and 600 K using meteorological data from the UK MetOffice (UKMO). The potential vorticity is used to select the SCIAMACHY measurements made inside the vortex. In this study 38 PVU of modified potential vorticity was used to define the edge, with $1 \text{ PVU} = 1 \times 10^{-6} \text{ K m}^2 \text{ kg}^{-1} \text{ s}^{-1}$. Having sampled all measurements within the polar vortex, they were then averaged to produce a daily vortex mean. Diabatic descent rates for each measurement were then calculated and also averaged. From the vortex mean diabatic descent, the dynamical ozone supply to the vortex mean ozone at a given isentropic level is calculated. At the end of the winter–spring the sum of the “measured” ozone loss (observed ozone difference between starting date and end date) and the accumulated dynamical supply yields the net chemical ozone loss at a given isentrope. Measurements of optical spectrometers as SCIAMACHY, GOME, or GOME-2 are made only in sunlit parts of the vortex. The coverage of the vortex at the

Title Page

Abstract

Introduction

Conclusions

References

Tables

Figures

◀

▶

◀

▶

Back

Close

Full Screen / Esc

Printer-friendly Version

Interactive Discussion



The Arctic low ozone period 2011R. Hommel et al.

[Title Page](#)[Abstract](#)[Introduction](#)[Conclusions](#)[References](#)[Tables](#)[Figures](#)[◀](#)[▶](#)[◀](#)[▶](#)[Back](#)[Close](#)[Full Screen / Esc](#)[Printer-friendly Version](#)[Interactive Discussion](#)

beginning of the year after sunrise is thus somewhat sparse. Closer to the end of the vortex lifetime in early spring, parts of the vortex are observed more than once during one day and the vortex can also be probed at different local times. While the local time of the SCIAMACHY measurements inside the Arctic polar vortex is close to 11:00 LT in January, it changes during winter and spring and can reach around 19:00 LT at the beginning of April for measurements near the pole. This is not considered to be a limitation for the determination of the ozone loss, as the diurnal variation of O_3 within the vortex at a given potential temperature is negligible. This is not the case for the interpretation of the NO_2 and BrO within the vortex as these species have significant diurnal variations.

In addition to the vortex edge criteria ($PV > 38$ PVU) to select the measured profiles for vortex-averaging, we consider only measurements made south of 80° N. This is done in order to retain accuracy with respective model estimates, because its relatively coarse gridding makes the model's local time on SCIAMACHY overpass unprecise near the poles. This ensures that the comparisons of vortex-mean O_3 and its loss estimates are made under approximately equal conditions.

Unlike O_3 , BrO and NO_2 fields may be affected by strong diurnal variations. SCIAMACHY measurements are moving closer to the pole during the course of the winter–spring period because of the rising sun. Thus spring-time vortex-averages may be compiled from different local times, as for the higher latitudes there are 2–3 orbits crossing the same geolocation. Even if the overall number of profiles considered in the averages steadily increases with time – thus making the vortex-averages more representative – the uncertainty of the inferred vortex-average BrO and NO_2 time-series will slightly increase by 5–15 % when the vortex weakens during polar spring.

2.8 Chemistry transport model

For this study, an isentropic three-dimensional CTM (B3DCTM) with 29 levels between 330 and 2700 K (about 10 to 55 km) and a horizontal resolution of $2.5^\circ \times 3.75^\circ$ in latitude and longitude has been used (Sinnhuber et al., 2003; Aschmann et al., 2009,

The Arctic low ozone period 2011R. Hommel et al.

[Title Page](#)[Abstract](#)[Introduction](#)[Conclusions](#)[References](#)[Tables](#)[Figures](#)[◀](#)[▶](#)[◀](#)[▶](#)[Back](#)[Close](#)[Full Screen / Esc](#)[Printer-friendly Version](#)[Interactive Discussion](#)

2011). The model is driven by horizontal wind fields and temperature provided by the ERA-Interim reanalysis of the European Centre for Medium-Range Weather Forecasts (ECMWF). The chemistry scheme comprises 59 tracers and about 180 gas phase, heterogeneous and photochemical reactions and is an extended version of the SLIMCAT model described by Chipperfield (1999). Updates and improvements of the model set-up have been reported in Sinnhuber et al. (2003) and Winkler et al. (2008). Reaction rates and absorption cross sections are taken from the Jet Propulsion Laboratory (JPL) recommendations (JPL/NASA, 2006). An equilibrium treatment of polar stratospheric cloud (PSC) formation, including liquid aerosols, solid nitric acid tri-hydrate (NAT) and ice particles is implemented within the model.

The model run used in this study is a continuation of the original 21 yr integration presented in Aschmann et al. (2011). However, unlike the previous runs the vertical transport is derived from interactively calculated diabatic heating rates using the MIDRAD scheme (Shine, 1987). Identical to Aschmann et al. (2011), the model contains an additional 5 pptv of very short-lived halogen source gases. The model integrations start on June 2009/2010 running until April of the next year.

To assess the chemical ozone loss, we added an additional quasi-passive ozone tracer which is initialized with the standard ozone tracer. This is not completely passive but uses an adapted version of the linearized chemistry scheme LINOZ (McLinden et al., 2000; Kiesewetter et al., 2010b). This is to capture the impact of the large-scale ozone photochemistry independently from the main chemistry scheme. As the linearized scheme does not contain any parametrization for heterogeneous chemistry, the difference between the quasi-passive and the standard ozone tracer reveals the desired information about the chemical loss caused by heterogeneous multiphase processes. Similarly to the approach used to infer vortex-averaged ozone losses from SCIAMACHY limb measurements, for the calculation of model vortex-averages only those grid cells are taken into account where the modified potential vorticity exceeds 38 PVU at latitudes below 80° N, and where the solar zenith angle is between 75° and 88° on local time of SCIAMACHY overpass.

the following winter 2010/2011, polar stratospheric temperatures were lower favouring conditions for large polar ozone losses. The Arctic winter 2009/2010, one year before, is located at the upper end of the range of winter planetary wave activity (Fig. 3). In that winter the Brewer–Dobson circulation was particularly strong (coinciding with an extremely negative Arctic Oscillation phase) with very high ozone throughout the NH (Steinbrecht et al., 2011).

3.2 Arctic ozone in March 2010 and 2011

The consecutive winters 2010 and 2011 are good examples of largely varying ozone levels over the Arctic. In winter–spring 2010, Arctic ozone was unusually high, whereas a year later the so far largest ozone losses over the Arctic have been reported (e.g. Steinbrecht et al., 2011; Manney et al., 2011). Figure 4 compares partial columns of March mean stratospheric ozone in 2010 and 2011 from SCIAMACHY and GOME-2 with results from the isentropic Bremen CTM. In March 2010 and 2011 ozone was maximum above the North American and West Siberian landmasses, with minimum ozone found above the North Atlantic sector between Greenland and Scandinavia. In March 2010, even near the pole total ozone was very high, an effect which is attributed to the poleward meridional transport of ozone rich air from lower latitudes because at that time, the vortex had already collapsed. In 2011, the vortex was pretty stable until mid-March, so that ozone was largely depleted north of approximately 75° N. In particular with respect to GOME-2, the model reproduces well the observed c-shape pattern of the high ozone in the collar region and the low ozone over the Northern Atlantic and Europe.

From GOME-2 total ozone the Fortuin and Kelder (1998) climatology of tropospheric ozone was subtracted in order to obtain a comparable partial ozone column for the stratosphere. The model's lower boundary coincides with the lowest altitude retrieved from SCIAMACHY limb-scatter ozone measurements (~ 10 km), also the top of atmosphere is approximately equal to the highest altitude for which ozone was retrieved from limb, so that these two data products do not substantially differ in their vertical

Title Page

Abstract

Introduction

Conclusions

References

Tables

Figures

◀

▶

◀

▶

Back

Close

Full Screen / Esc

Printer-friendly Version

Interactive Discussion



The Arctic low ozone period 2011

R. Hommel et al.

Title Page

Abstract

Introduction

Conclusions

References

Tables

Figures

◀

▶

◀

▶

Back

Close

Full Screen / Esc

Printer-friendly Version

Interactive Discussion



extent, hence their vertical columns, as in Fig. 4, are directly comparable. With this in mind, and considering that ozone above 55 km contributes to around 0.1 % or less to the total column, it turns out that the model has an approximately 10 % positive bias in the stratospheric ozone column, compared to SCIAMACHY limb measurements. This bias is primarily reflected in high ozone values over the landmasses north of 40° N. In contrast, the model shows a good agreement with the two instrument's data in regions where column ozone is low. Sensitivity studies have shown that the modelled ozone column in the two years may vary by approximately 10 % depending on the approach used to model the vertical transport of stratospheric trace constituents. Results presented in this work are confined to model runs conducted with interactive heating rate calculations (MIDRAD), though apparent polar column ozone is larger than in simulations with prescribed ERA-Interim heating rates. The latter shows approximately 10 % lower column ozone in the collar region between 40° N and 70° N in both winter–spring periods. Although this better agrees with SCIAMACHY limb total ozone, modelled ozone profiles, respectively losses, which are in the focus of this study, are better represented in the interactive model.

The bias between GOME-2 and SCIAMACHY can most likely be attributed to the relatively simple approach used to obtain a stratospheric column from the measured GOME-2 total column.

3.3 SCIAMACHY limb measurements: O₃, NO₂ and BrO

Individual chemical processes governing ozone losses in the Arctic stratosphere are difficult to measure directly and independently from dynamical processes which largely determine the interannual variability of polar ozone and its synoptic day-to-day changes. In the following, we use correlative SCIAMACHY limb observations to illustrate the temporal development of ozone and related chemical constituents in the winter–spring Arctic vortex 2010 and 2011, each being representative of a warm and cold Arctic winter stratosphere, respectively. Chemically-induced ozone losses are inferred

from limb measured ozone mixing ratio profiles (Eichmann et al., 2002; Sonkaew et al., 2013).

3.3.1 Vortex-averages

Figure 5 shows the temporal evolution of the vortex-averaged observed ozone mixing ratio from January to April in 2010 and 2011. It also depicts the evolution of the SCIAMACHY limb-scatter measured and vortex-averaged BrO and NO₂ mixing ratios, two gases, which are largely being involved in the chemical cycles destroying ozone. In 2011 below the 525 K isentropic level O₃ was as low as 0.5–1.5 ppmv after 12 March 2011 until the vortex became unstable and broke down. Differences in the vortex dynamics in the two years explain the obvious differences seen in the ozone time-series above 550 K: in 2010, when the vortex was much weaker than in 2011, the variability in the ozone profiles is quite large in the upper layers. Higher temperatures in a weaker vortex 2010 go along with a higher variability in the descent of air from above (descent is stronger in weaker vortices; Rosenfield et al., 1994), contributing to the variability at the ozone mixing ratio maximum within the vortex. The vortex mean ozone in Fig. 5 highlights another, not previously investigated detail in the ozone mixing ratios: a sudden reduction of ozone down to 1.5 ppmv or less occurred during an eight-day period, commencing 21 January 2011. In Sect. 3.8 this episode and its origins are examined.

The interannual variability of BrO increases with latitude as shown by Sinnhuber et al. (2002) using observed and modelled stratospheric BrO slant column densities. For the measurement site at Ny-Ålesund (79° N, 12° E) they showed winter-to-winter deviations of up to 40 %. Stations further south exhibited weaker year-to-year changes. Since stratospheric BrO is produced in the tropics from short- and long-lived source gases (WMO, 2010), polar BrO levels depend, like ozone, on the strength of the large-scale meridional transport linked to the planetary-scale wave activity. The BrO vortex-averaged time-series of Fig. 5 are giving us the impression that in the depicted period 2011 the BrO variability was somewhat larger than in 2010. In particular before 15 March 2011 also the overall mixing ratio level is 1–2 pptv lower than in 2010. The latter

Title Page

Abstract

Introduction

Conclusions

References

Tables

Figures

◀

▶

◀

▶

Back

Close

Full Screen / Esc

Printer-friendly Version

Interactive Discussion



is confirmed by polar maps of the stratospheric BrO partial column, constructed from 6 day running means of the SCIAMACHY limb measurements (not shown). The pronounced temporary minimum in the BrO mixing ratio below 550 K seen in late January 2011 is clearly associated with low ozone values – this relationship is also examined in Sect. 3.8.

In April of the two years, the vortex-mean BrO abundance drops quickly. This is because the vortex is becoming unstable and to a certain degree allows BrO poor air from mid-latitudes to be mixed into the vortex. During spring the near-polar BrO mixing ratio decreases relatively rapidly by approximately a third, an effect which is pronounced in the lowermost stratosphere below 20 km (~ 475 K; Theys et al., 2009). Also, in spring and summer the positive vertical gradient in the near-polar stratospheric BrO mixing-ratios is weaker than during the winter month (e.g. McLinden et al., 2010).

During polar night most of the stratospheric NO_x is converted into reservoir species, mainly N_2O_5 and HNO_3 . NO_x , hence NO_2 , will be recycled when sunlight returns in late-winter and spring. This is clearly seen in the vortex-average NO_2 mixing ratios from SCIAMACHY limb measurements (Fig. 5). Below the 550 K isentrope, NO_2 is below 0.1 ppbv throughout January. The replenishment of vortex NO_2 in winter–spring 2011 is substantially delayed when compared to 2010 conditions. The long-lasting stable vortex delays horizontal mixing of NO_2 -rich air from mid-latitudes into the vortex, as shown by Konopka et al. (2007) for the 2002/2003 Arctic winter. Secondly, in a strong vortex less air from the mesosphere and upper stratosphere (where NO_x is available or even formed during the course of the winter) descends into lower polar stratosphere. Additionally, in winter–spring 2011 PSCs effectively denitrified the Arctic stratosphere as never observed before (Manney et al., 2011; Khosrawi et al., 2012, see Sect. 3.6), keeping NO_2 levels low in lower regions of the vortex until the end of March 2011 (compare NO_2 from SCIAMACHY nadir measurements, Fig. 10b).

The Arctic low ozone period 2011

R. Hommel et al.

[Title Page](#)[Abstract](#)[Introduction](#)[Conclusions](#)[References](#)[Tables](#)[Figures](#)[I◀](#)[▶I](#)[◀](#)[▶](#)[Back](#)[Close](#)[Full Screen / Esc](#)[Printer-friendly Version](#)[Interactive Discussion](#)

3.3.2 Inferred ozone losses

By applying the vortex-averaging method of Eichmann et al. (2002) to SCIAMACHY limb-scatter ozone profiles, we estimate a chemically-induced ozone loss below the 550 K isentropic surface of up to 77 % in April 2011, relative to values measured the first day of the year (bottom panel of Fig. 5). Even in the short period between 21 and 29 January 2011, we infer an ozone reduction by 60 % on average, which quickly recovered afterwards. It is known that such rapid ozone reductions and subsequent recoveries are pure dynamical features, typically caused by so-called ozone mini-hole events (e.g. Weber et al., 2002). Why this is influencing an isentropic ozone loss estimate, developed to infer the strength of the chemically-induced polar ozone destruction independently from reasons related to the dynamics of the atmosphere, is examined in more detail in Sect. 3.8.

By comparison, in the warmer and weaker Arctic vortex 2010 ozone losses barely exceeded 20 % below 550 K. Above the 550 K isentropic surface, however, we infer an ozone depletion of up to 40 % during spring 2010 (relative to values at first day of the year). The slower descent of air in the strong vortex 2010/2011 implies that this upper layer of ozone depletion is found at higher altitudes as in 2010. Above the regions where halogen driven catalytic cycles remove ozone, NO_x ($\text{NO} + \text{NO}_2$) photochemistry is predominantly responsible for ozone depletion (Osterman et al., 1997). This process is stronger during warm winter years when the vortex is weaker because less denitrification on fewer PSCs is taking place, air from the upper stratosphere is faster descending and the lateral mixing of NO_2 -rich air from mid-latitudes is more likely than in cold winter–spring periods when vortex mixing-barrier is much stronger (Rosenfield et al., 1994; Konopka et al., 2007). As shown in Sonkaew et al. (2013) these NO_x driven catalytic ozone losses above the 550 K isentropic level are frequently observed in the Arctic polar stratosphere in late spring.

Manney et al. (2011) reported chemically induced ozone losses on the order of at least 2.5 ppmv between 470 K and 550 K by end of March 2011 from Lagrangian

Title Page

Abstract

Introduction

Conclusions

References

Tables

Figures

◀

▶

◀

▶

Back

Close

Full Screen / Esc

Printer-friendly Version

Interactive Discussion



The Arctic low ozone period 2011

R. Hommel et al.

[Title Page](#)[Abstract](#)[Introduction](#)[Conclusions](#)[References](#)[Tables](#)[Figures](#)[◀](#)[▶](#)[◀](#)[▶](#)[Back](#)[Close](#)[Full Screen / Esc](#)[Printer-friendly Version](#)[Interactive Discussion](#)

chemical transport model studies and ozone measurements from MLS/Aura and the Match network of ozone sondes. This number is consistent with ours, which is 2.5–3 ppmv at the end of March. Our SCIAMACHY based loss estimate, however, is slightly (0.5 ppmv) lower above 525 K as that of Manney et al. (2011). The onset of the catalytic ozone destruction occurs around 1 February 2011 in both studies. Sinnhuber et al. (2011) inferred column ozone losses of up to 120 DU towards end of April 2011 from MIPAS observations. These observations are principally confirmed by corresponding model simulations conducted with an isentropic CTM of very similar set-up as ours used in this study (Sinnhuber et al., 2003; Aschmann et al., 2011), but differently initialized and driven by meteorology from the ECMWF operational analysis. Sinnhuber et al. (2011) also showed MIPAS ozone at the 475 K isentropic surface reduced to 1.5 ppmv in early April 2011, which is rather at the upper end of our estimate. Arnone et al. (2012) reported MIPAS based vortex-averaged ozone reductions down to 0.6 ppmv in early April 2011 at 18 km (\sim 430 K isentrope), in good agreement with our data. Their corresponding ozone losses are also matching our estimates, although based on a different method, taking correlative MIPAS N₂O observations into account.

3.4 SCIAMACHY solar occultation measurements: O₃, NO₂ and BrO

In order to complement our results obtained from the limb-scatter measurements shown in Fig. 5, we also retrieved O₃, BrO, and NO₂ profiles from SCIAMACHY solar occultation measurements (Fig. 6). As for limb profiles, in our analysis we consider only those occultation profiles located within the vortex. Since solar occultation measurements were performed at different local time (sunset around 18:00 LT, compared to morning local time around 10:00 LT for limb geometry), respective vortex-averages are obtained from different geolocations compared to the limb data. This is demonstrated clearly in Fig. 7, which shows 475 K potential vorticity maps for two days during winter 2011 together with geolocations of limb and solar occultation measurements. The vortex edge is approximately at 38 PVU, here indicated by yellow contour shades. Occultation measurements are the larger grey coloured circles, limb measurements

The Arctic low ozone period 2011R. Hommel et al.

[Title Page](#)[Abstract](#)[Introduction](#)[Conclusions](#)[References](#)[Tables](#)[Figures](#)[◀](#)[▶](#)[◀](#)[▶](#)[Back](#)[Close](#)[Full Screen / Esc](#)[Printer-friendly Version](#)[Interactive Discussion](#)

are the smaller dots. White limb dots mark measured profiles outside the vortex, those considered in the vortex-averages are marked in black. On 23 February the vortex is nearly concentric and close to the pole (stable vortex). On this day only four solar occultation profiles, from locations over Central Siberia contribute to the time-series shown in Fig. 6, compared to 130 profiles in limb-scattering geometry. On 15 April, the situation is very different. The vortex is largely displaced towards Central Siberia, stretching down to regions over South-Eastern Europe. During that day most limb profiles are concentrated near the pole, only a few limb profiles capture the vortex region south of 70° N. In that case five solar occultation profiles lie within the vortex, and not necessarily close to its edge as on 23 February 2011.

It is important for comparing the constructed solar occultation measured BrO and NO₂ vortex-averages with the limb observation results (Fig. 5), that the local time of the solar occultation measurement is quite different from the limb measurement. Both gases have a strong diurnal cycle, with steepest gradients appearing at sunrise and sunset. Solar occultation measurements are performed during local sunset so that we cannot rule out that the obtained vortex-averaged time-series of the two gases may illustrate a different state of the vortex with respect to daytime limb measurements. BrO mixing ratios may be lower than during mid-day, NO₂ larger, since the diurnal cycle of the two gases are highly anti correlated (Lary et al., 1996). Evident in the solar occultation time-series are larger mixing ratios in particular in BrO and NO₂ compared to limb (Fig. 5). O₃ mixing ratios are only slightly larger above the 625 K isentrope (~ 25 km). That is because occultation profiles are obtained at lower latitudes as limb profiles, so that the measurements are generally conducted over the landmasses of the Northern Hemisphere where the column amount of the three species is largest.

Qualitatively the temporal evolution of the time-series obtained from limb-scatter and solar occultation measurements are quite similar. But also interesting differences are seen. Although the variability of the occultation measured mixing ratios in comparison to limb vortex-averages is larger in the upper layers and in spring when the large ozone losses occur, but the low ozone period commencing 21 January 2011 is not seen in

the occultation time-series. However, noticeable small O_3 mixing ratios are seen at the 400 K isentropic surface also in January and February. These sporadically occurring events may be influenced by mixing processes with tropospheric air stirred into the lowest regions of the vortex (limb data were not processed at this isentrope).

The time-series of averaged BrO and NO_2 profiles from solar occultation measurements show approximately a factor two larger mixing ratios as limb vortex-averages. Together with a noticeably larger variability of the two time-series from the solar occultation measurements this clearly results from the sparse sampling over the vortex area, more or less along its edge, where the mixing ratios are per se larger than further poleward. Along the edge a certain probability of horizontal stirring with air from mid-latitudes exists that may be captured in the occultation measurements. Hence solar occultation averages as shown here are not representative for inner vortex conditions.

3.5 Reproducing limb-observations of O_3 , NO_2 and BrO using the Bremen-CTM

3.5.1 Modelled vortex-averages

From the stratospheric isentropic Bremen-CTM we constructed vortex-averages for O_3 , BrO and NO_2 in a similar way as for the limb observations (Fig. 8). For each isentropic model level between 419 K and 662 K we averaged only over those grid cells south of 80° N where the modified PV was larger than 38 PVU (indicating the vortex edge) and the solar zenith angle during SCIAMACHY overpass was between 75° and 88° . As seen from Fig. 8, the timing of the onset of decreasing ozone mixing ratios as well as layers where this decrease occurs, below the 550 K isentropic surface, are well reproduced in 2011. However, ozone drops below 1.5 ppmv one week earlier in the model around 5 March. In the observations this is seen around 12 March 2011 (Fig. 5). Above 550 K, the CTM tends to overestimate ozone in the vortex. The period of low O_3 below 550 K in mid-January 2011 is not reproduced in the CTM – we are examining this in more detail also in Sect. 3.8.3. Also the situation in 2010 is well reproduced by the model, though with a weaker variability.

Title Page

Abstract

Introduction

Conclusions

References

Tables

Figures

◀

▶

◀

▶

Back

Close

Full Screen / Esc

Printer-friendly Version

Interactive Discussion



The Arctic low ozone period 2011R. Hommel et al.

[Title Page](#)[Abstract](#)[Introduction](#)[Conclusions](#)[References](#)[Tables](#)[Figures](#)[◀](#)[▶](#)[◀](#)[▶](#)[Back](#)[Close](#)[Full Screen / Esc](#)[Printer-friendly Version](#)[Interactive Discussion](#)

The temporal development of vortex BrO in the model differs from SCIAMACHY limb observations in several ways: modelled BrO profiles in the vortex are biased low in both years, in particular at lower isentropes. Above 550 K, this low bias is on the order of ~ 2 pptv during mid-winter, increasing to ~ 5 pptv later in March. Also, modelled BrO decreases gradually with time until polar BrO is getting low due to the break-up of the vortex later in spring. A similar gradual decrease is not seen in the limb data. In contrast, limb BrO is high in February and March of both years, suggesting to decrease relatively rapidly within a week or so, when the vortex becomes unstable. Limb-measured BrO in the vortex is also somewhat lower in mid-winter 2011 than in 2010, presumably due to slower large-scale meridional transport from the regions of its photochemical production. Although this assumption is supported by the modelled O_3 and NO_2 , whose levels are also generally slightly lower in 2011 than in 2010, modelled BrO is 1–2 pptv larger above 475 K in 2011 than in the year before. This effect might be partly explained by a shift in the chemical equilibrium of the formation reaction of bromine nitrate ($BrONO_2$) towards BrO due to the lower NO_2 mixing ratios.

With the return of sunlight, polar NO_2 is reconverted from its reservoir species N_2O_5 . Although the timing of the onset of this photochemical regeneration is well reproduced by the CTM, springtime vortex-averaged NO_2 levels are underestimated. This underestimation results from a generally low bias in model NO_2 , so that lateral mixing of NO_2 -rich air from mid-latitudes (Noxon cliff; Noxon, 1979) cannot account for restoring springtime polar NO_2 levels to the same extent as seen in the limb vortex-averages. In April 2011, the CTM shows approximately half of the NO_2 measured by SCIAMACHY limb, in April 2010 the low bias is less distinct and in the order of a third.

3.5.2 Modelled ozone losses

In the model, polar ozone losses are quantified as the difference between the modelled chemically fully interactive ozone and a quasi-passive ozone tracer (LINOZ; linearised chemistry without heterogeneous reactions). Resulting losses are in good agreement with the estimate from SCIAMACHY limb measurements below the 550 K isentropic

The Arctic low ozone period 2011

R. Hommel et al.

[Title Page](#)[Abstract](#)[Introduction](#)[Conclusions](#)[References](#)[Tables](#)[Figures](#)[◀](#)[▶](#)[◀](#)[▶](#)[Back](#)[Close](#)[Full Screen / Esc](#)[Printer-friendly Version](#)[Interactive Discussion](#)

surface. Relative to SCIAMACHY, modelled ozone losses are approximately 10 % over-estimated in April 2011. In 2010, we find rather a slightly underestimation of the modelled induced losses in that region. The overestimation of the 2011 loss is in the same range as the ones reported by Singleton et al. (2007) from SLIMCAT CTM model studies of the so far most severe Arctic ozone losses observed in winter–spring 2004/2005. They compared to loss estimates from various satellite instruments based on the passive tracer subtraction method and argued that mainly sampling differences between the data sets may have led to overestimated model losses. The differences between the ozone loss inferred from our CTM simulations and the estimates from SCIAMACHY limb measurements are also partly attributable to small differences in the vortex sampling of the two data sets. Additionally, we cannot rule out that deficits in the model treatment of PSCs and accompanied effects of heterogenous chemistry on those particles may play a substantial role in the overestimation of ozone depletion, in particular during spring.

One striking difference between ozone losses from SCIAMACHY and the CTM is the absence of the NO_x driven ozone decomposition layer above 550 K in the model. This is not an effect of the general underestimation of polar NO_2 in the CTM, it is rather an inherent effect of the approach used to infer ozone losses in the model. The loss due to NO_x is parameterized in the LINOZ scheme and thus impacts the linearized ozone tracer which represents the reference of the model's loss estimate. Consequently, this layer is not deducible from the approach used here.

The apparent ozone loss in mid-January 2011 seen in the SCIAMACHY limb estimate (Fig. 5, bottom right panel), however, is also not inferable from model results since a respective decrease of ozone mixing ratios is not seen in the modelled ozone time-series. In Sect. 3.8.3 we investigate this behaviour in more detail.

3.6 SCIAMACHY limb observations of PSCs

The meteorological conditions in the 2011 Arctic winter–spring polar vortex favoured the formation of PSCs. Figure 9 shows the temporal evolution of the daily mean PSC

The Arctic low ozone period 2011

R. Hommel et al.

Title Page

Abstract

Introduction

Conclusions

References

Tables

Figures

◀

▶

◀

▶

Back

Close

Full Screen / Esc

Printer-friendly Version

Interactive Discussion



occurrence rate (left panel) and daily averaged PSC altitude (right panel) – both in the 60° N–80° N latitude range – for several Arctic winters including 2010/2011 from 1 January to 1 April. The PSC occurrence rate is given by the ratio of the number of SCIAMACHY measurements with PSC detections and the total number of measurements – on a given day and within a certain latitude range.

In January 2010 a very strong PSC occurrence during an approximately one-month period, from mid-December to mid-January seen in Fig. 9, was observed also by the space-borne CALIOP (Cloud-Aerosol Lidar with Orthogonal Polarisation) instrument onboard CALIPSO (Cloud-Aerosol Lidar and Infrared Pathfinder Satellite Observations) as shown in Khosrawi et al. (2011) and Pitts et al. (2011). The total supply of PSCs during the entire winter–spring period was even stronger in 2011. From SCIAMACHY limb-scatter observations we infer that the PSC occurrence rate in 2010 was some 20 % larger than in 2011, but only during a relatively short period, that ended at the beginning of February 2010. In contrast, during the 2010/2011 season, PSCs were formed from the end of December 2010 and were present over the pole until the 18th of March (Khosrawi et al., 2012).

The 2011 SCIAMACHY PSC record shows three periods of maximized PSC formation – at the beginning of January, from 18 January to 1 February and a long-lasting period after the 8 February. During this third period, the PSCs occurrence rate steadily increased, until a maximum was observed on 22 March 2011. In comparison, CALIOP detected four PSC periods, starting earlier on 23 December 2010. Not exactly similar to the periods seen by SCIAMACHY, but largely overlapping. A similar increase during March was also observed in 2005, when the so far largest total ozone mass loss was observed (Sonkaew et al., 2013). In 2005, however, most PSCs were formed during the last days of January – at comparable rates as in 2008 and 2010. In the latter two years, however, respective periods lasted only a few days, hence were distinctly different from the conditions seen in 2011 and 2005.

In this context, we also have to keep in mind that the vortex sampling of SCIAMACHY limb measurements in January may be quite poor, and the variability in PSC occurrence rates seen in Fig. 9 in January may be partly explained by this.

The right panel of Fig. 9 impressively demonstrates the PSC descent during the course of winter–spring. This descent is not only attributed to particle sedimentation, to a large extent it reflects the descent of the lower stratospheric temperature minimum, as has been demonstrated for the Southern Hemisphere by von Savigny et al. (2005a). PSC altitudes derived from SCIAMACHY correspond to PSC top altitudes, not to centroid altitudes. The cloud thickness cannot be inferred using the method applied.

Informations about the composition of the observed PSCs can be obtained from measurements by the CALIOP instrument onboard CALIPSO. According to CALIOP, the 2009/2010 PSC season started with the formation of predominantly type I PSCs, that diverged more and more over time into the formation of type II (ice) particles. In contrast, during the whole 2010/2011 PSC season, type II clouds were always found together with type Ia (NAT) and type Ib (STS) clouds (Khosrawi et al., 2012). However, from such informations alone one cannot state which PSC type is giving rise to particular features or characteristics that are seen in the vortex-average ozone time-series. But PSC observations correlate well with certain aspects seen in the polar HNO_3 and N_2O time-series as measured by other instruments, for instance MLS/Aura or SMR/Odin (Khosrawi et al., 2011, 2012; Manney et al., 2011). Khosrawi et al. (2011) showed that the so far largest denitrification over the last decade in winter–spring 2009/2010 emerged from an extended formation of solid particles (NAT/ice) in early winter. In winter–spring 2011, the overall denitrification was even more pronounced than in the winter before. It lasted much longer over four months and developed rather continuously, in contrast to the rather short one-month period of cold temperatures in 2010 (Khosrawi et al., 2012). There is no doubt that denitrification played a large role for the ozone losses 2011, however, recently Strahan et al. (2013) argued that the unexpected dynamical situation of the polar stratosphere may be accountable for around one-third of the ozone destroyed in the Arctic vortex in March and April 2011.

The Arctic low ozone period 2011

R. Hommel et al.

[Title Page](#)[Abstract](#)[Introduction](#)[Conclusions](#)[References](#)[Tables](#)[Figures](#)[◀](#)[▶](#)[◀](#)[▶](#)[Back](#)[Close](#)[Full Screen / Esc](#)[Printer-friendly Version](#)[Interactive Discussion](#)

In 2005, when the so far largest Arctic chemical ozone losses were observed (Manney et al., 2006, 2011; Sonkaew et al., 2013), a temporal evolution of PSC occurrence is seen which is very similar to that in 2011.

After a strong event of PSC formation around 30 January 2005, PSCs were further formed over large areas over the Arctic, steadily increasing until the end of February when a final warming halted PSC existence. Based on model studies, Feng et al. (2007) argued that during the course of the 2005 winter PSCs were mainly composed of type I (STS/NAT), whereby the strong PSC formation around 30 January 2005 is attributable to type I and II PSCs in approximately equal measure.

3.7 Chlorine activation from SCIAMACHY in comparison with ground-based DOAS measurements

While OCIO is not directly involved in ozone depletion, it is formed by reaction of BrO and ClO which are both key substances in catalytic ozone removal. While BrO concentrations do not vary strongly from year to year, ClO concentrations do, making OCIO an indicator for chlorine activation.

As shown in Fig. 10a, OCIO slant columns at 90° SZA from SCIAMACHY nadir measurements vary strongly from year to year. After an initial increase in mid-December, the values remain elevated in January and then decrease until the end of the observation period in mid-March, when no more 90° SZA measurements are available in the ascending part of the orbits. In some years, OCIO levels remain elevated until beginning of March, while in other years, activation already ends in January. The cold winter in 2010/2011 was unique in that OCIO values remained high until the end of observations, indicating persistent chlorine activation. The observed large variability in OCIO columns is mainly explained by interannual differences in chlorine activation, resulting from differences in stratospheric temperatures and PSC formation rates. Some additional variability is introduced by the satellite observation method at 90° SZA which is limited to a certain latitude range for each day. Depending on the size and deforma-

Title Page

Abstract

Introduction

Conclusions

References

Tables

Figures

◀

▶

◀

▶

Back

Close

Full Screen / Esc

Printer-friendly Version

Interactive Discussion



tion of the polar vortex, this can lead to variations in the sampling of the region with activated chlorine.

NO_2 is involved in both, the catalytic destruction of ozone and in the formation of reservoir species such as chlorine nitrate (ClONO_2). Daytime levels of NO_2 are mainly determined by day length which governs the partitioning between NO , NO_2 , and its reservoirs, and to a lesser degree by temperature. During polar night, it is converted into N_2O_5 and HNO_3 which can be incorporated into PSCs and thereby be removed from the gas phase. Usually, this removal is reversible as PSCs evaporate, but if PSCs sediment to lower altitudes, persistent denitrification of some atmospheric layers can occur. The removal of NO_2 is of particular importance for the length of stratospheric chlorine activation as in its absence, the formation of inactive chlorine reservoirs is delayed.

In general, the variability in the NO_2 columns is relatively small, mainly because day length is the determining factor. This is illustrated in Fig. 10b, where SCIAMACHY NO_2 columns are shown for a number of Arctic winters. The main difference between individual years is the onset of the recovery of NO_2 columns in spring, and no clear link between years with large chlorine activation and those with late onset of NO_2 increase is apparent. However, the cold winter 2010/2011 differs from all previous winters in that no sign of increase in NO_2 columns is observed until the end of the observation period, and NO_2 levels are at a record low for every single day after 15 February. In agreement to other satellite observations shown by Manney et al. (2011) and Khosrawi et al. (2011), this indicates that in spring 2011 NO_y was removed from the lower Arctic stratosphere by large scale denitrification, providing the conditions for strong and persistent ozone depletion.

Also ground-based DOAS measurements in Ny-Ålesund (79°N , 12°E ; Fig. 10c and d) confirm that the winter–spring 2011 was exceptional compared to other years with strong chlorine activation, like 2005 and 2008. As already seen in the SCIAMACHY observations, the winter 2010/2011 was unique in that OCIO values remained high until the end of observations shortly after the 20th of April. Significant levels of OCIO well

The Arctic low ozone period 2011

R. Hommel et al.

Title Page

Abstract

Introduction

Conclusions

References

Tables

Figures

◀

▶

◀

▶

Back

Close

Full Screen / Esc

Printer-friendly Version

Interactive Discussion



above the detection limit have been detected until the beginning of April, indicating chlorine activation about four weeks later in the year than in previous years. For NO₂ the results are similar: very low levels indicating efficient denitrification has been seen from the ground-based observations until April 2011 as well.

3.8 Low Arctic ozone in January 2011

The SCIAMACHY limb time-series of vortex-averaged Arctic ozone (Fig. 5) exhibits two periods of low ozone in winter–spring 2011, as discussed in Sect. 3.3. In addition to the long-lasting, chemically-induced ozone depletion in March and April, for several days commencing 21 January 2011 ozone mixing ratios in the Arctic vortex dropped on average to values less than 1.5 ppmv below the 500 K isentrope. When the ozone loss, relative to values on the first day of year, is inferred from this time-series via the vortex-averaging method of Eichmann et al. (2002), the January 2011 low ozone episode seems also attributable to chemical depletion caused by ODS, similarly as the long-lasting low ozone period in March and April 2011. Even if enough ODS were activated by then, it would need some time to chemically destroy most of the ozone in a relatively thick layer of the vortex, so that this mechanism alone cannot explain such a sudden drop in the vortex ozone mixing ratios. Also, why then should ozone recover a few days later at approximately the same rate when a strong mixing barrier encompassing the vortex prevents exchange with surrounding ozone-rich air?

In the most recent studies examining the strength and causes of the 2011 Arctic ozone hole, the period of low ozone in January 2011 was not investigated in greater detail, since most of the studies focused on the severe chemically-induced ozone losses later in that year (Hurwitz et al., 2011; Sinnhuber et al., 2011; Balis et al., 2011; Arnone et al., 2012; Manney et al., 2011). Therefore, in the following we are attempting to examine the causes leading to the so far briefly discussed transient low ozone period in January 2011 and examine why this feature is not seen in the inferred ozone losses from chemistry transport model calculations.

The Arctic low ozone period 2011

R. Hommel et al.

Title Page

Abstract

Introduction

Conclusions

References

Tables

Figures

◀

▶

◀

▶

Back

Close

Full Screen / Esc

Printer-friendly Version

Interactive Discussion



3.8.1 Observations and meteorological situation

In Fig. 11 a twelve-day sequence of nadir-scanned GOME-2 total ozone is shown, beginning on 20 January 2011, one day before low column ozone was observed over Central Siberia north of Sakhalin island. This area of low ozone was centered at approximately 140° E/ 63° N and had an initial extent of about $2000 \text{ km} \times 1000 \text{ km}$ in longitude and latitude (or $1.4 \times 10^6 \text{ km}^2$). In the following six days the low ozone area approximately doubled in size and moved westwards across the Ural region. On 28 January it moved a few degrees eastwards towards Central Siberia, where it dissolved two days later. Thereafter, Arctic ozone replenished temporarily until around the 6 February. Vortex ozone again declined and remained low for the following almost three month, according to the SCIAMACHY limb vortex-averaged O_3 mixing-ratio time-series (Fig. 5). This temporarily effect is very typical for so-called ozone mini-hole events which are caused by intrusion of subtropical air masses with a high tropopause (Weber et al., 2002).

Although before 21 January 2011 PSCs were present in the Arctic stratosphere (Fig. 9), until then, not much chlorine had been activated (Fig. 10) that could have led to substantial chemical ozone destruction in mid-January. Hence, such a sudden drop and subsequent rapid recovery of polar ozone can only be explained by dynamical changes.

For quite some time now, sporadically occurring extreme total ozone events on synoptic scales related to weather regimes in the upper troposphere and tropopause region have been investigated (e.g. Reed, 1950). Those events have been named “ozone mini-holes” (OMH; Newman et al., 1988). Based on TOMS total ozone observations since 1979, James (1998) found a strong connection between the occurrence of OMHs and the storm-track regions in the North Atlantic and North Pacific and noted a considerably larger frequency of OMH formation during January to March, with a tendency to later formation the further north the hole appears in the Northern Hemisphere. OMHs are caused in the stratosphere when the tropopause is elevated as a consequence of

Title Page

Abstract

Introduction

Conclusions

References

Tables

Figures

◀

▶

◀

▶

Back

Close

Full Screen / Esc

Printer-friendly Version

Interactive Discussion



advection of sub-tropical air moving poleward during the passage of upper tropospheric anticyclones (Krzyściń, 2002). This also implies a lifting of isentropic surfaces above the anticyclonic ridges, which in turn leads to horizontal divergence of ozone out of the stratospheric column, a quasi secondary effect of OMH formation as pointed out by Koch et al. (2005).

In recent years, investigations of mechanisms leading to OMH formation in the Northern Hemisphere focussed on the Northern Atlantic storm track regions where mini-holes are formed predominantly. For example, Weber et al. (2002) reported on an OMH formed in February 1996 above Greenland and at the vortex edge. Associated with it were very low stratospheric temperatures (below 188 K, sufficiently low for PSC II formation) and very low total ozone close to 180 DU. This OMH moved within a few days in northwest direction and dissipated north of Siberia.

Only a few studies investigated the relationship between OMHs observed over Central or Eastern Asia (where the January 2011 low ozone is found) and respective atmospheric conditions in those regions. While Liu et al. (2009) studied OMH conditions over the Tibetan Plateau in December 2003 and linked their occurrence to tropopause elevations associated with the poleward displacement of the subtropical jet triggered by deep tropical convective heating (Madden–Julian Oscillation), Han et al. (2005) found evidence for OMH formation during December 2001 associated with poleward motion of lower stratospheric air east of the Aleutian high. Both studies describe OMHs observed south of 40° N, not mentioning OMH conditions over Asia further poleward, as seen in January 2011. The mini-hole we are examining here formed initially over West Asian continental regions, clearly west of the Northern Pacific storm track which has been reported as another preferred region of OMH formation, in addition to the other preferred region over the North Atlantic (Orsolini et al., 1998). James (1998) identified an increased number of mini-holes occurrences over Central Siberia, at least 45° westward of the Northern Pacific storm track region, which agrees closely with the area where the OMH has been observed in January 2011. However, the authors neither

The Arctic low ozone period 2011

R. Hommel et al.

Title Page

Abstract

Introduction

Conclusions

References

Tables

Figures

◀

▶

◀

▶

Back

Close

Full Screen / Esc

Printer-friendly Version

Interactive Discussion



described where Central Siberian mini-holes were formed nor in which direction they move when formed near the date line.

Not only the pronounced poleward placement of the January 2011 ozone low is somehow remarkable with respect to its potential dynamical drivers as mentioned above, also a few other characteristics of this particular OMH appear exceptional: low total ozone over Asia has been observed for ten days in January 2011, which is substantially longer as the typical lifetime of ozone mini-holes (1–4 days; Newman et al., 1988). Krzyścin (2002) found OMH lifetimes longer than six days only during six years between 1926 and 1999. The maximum area of the January 2011 OMH is much larger than typical sizes observed in other events. Newman et al. (1988) refer to OMHs extending over 1000–3000 km (approx. 8×10^5 to 7×10^6 km²), whereas Koch et al. (2005) found that OMHs cover $\sim 5 \times 10^5$ km². While on the first day of appearance (21 January) the area of GOME-2 total ozone lower than 300 DU is not larger than 2000 × 1000 km, covering an area of approximately 1.4×10^6 km², during its largest extent on 27 January, the GOME-2 low ozone area covered a region of more than 3400 km zonally and 2000 km meridionally, or 3.5×10^6 km². Due to the limitations of satellite observations during daytime, the area of the OMH could have been even larger and well extending into the polar night. From our CTM simulations, which are capturing the evolution of this low ozone period in January 2011 quite well (Fig. 12), we obtain that on 27 January 2011 the true meridional extent of the OMH could be as large as its zonal extent, putting its area in the range of 1×10^7 km². This is almost a third larger than values given in literature referring to typical OMH sizes and almost as large as a typical area covered by an Antarctic ozone hole in southern hemispheric spring.

Also remarkable is the motion of the January 2011 low ozone area. In the first six days after being detected, it moved westward. In contrast, typical OMHs move in the opposite direction associated with the motion of anticyclones and the jet stream.

In order to examine whether the January 2011 low ozone event is attributable to tropopause disturbances similarly as OMHs, in Figs. 13–15 we further elucidate meteorological conditions near the tropopause. GOME-2 first detected lower ozone over

The Arctic low ozone period 2011

R. Hommel et al.

Title Page

Abstract

Introduction

Conclusions

References

Tables

Figures

◀

▶

◀

▶

Back

Close

Full Screen / Esc

Printer-friendly Version

Interactive Discussion



The Arctic low ozone period 2011R. Hommel et al.

[Title Page](#)[Abstract](#)[Introduction](#)[Conclusions](#)[References](#)[Tables](#)[Figures](#)[◀](#)[▶](#)[◀](#)[▶](#)[Back](#)[Close](#)[Full Screen / Esc](#)[Printer-friendly Version](#)[Interactive Discussion](#)

Eastern Siberia on 21 January 2011 (Fig. 11). In this region the vortex slid over a region where tropopause temperatures decreased below 205 K (Fig. 13) due to adiabatic cooling where the tropopause was elevated from motion of air passing an anticyclone in the upper troposphere. The tropopause lifting coincides with higher geopotential heights (Fig. 14). The imposed lifting of isentropes above the elevated tropopause in this region is also seen nicely in Fig. 15, where the atmospheric pressure decreases at the 350 K isentropic surface. The synoptic situation did not change until 25 January 2011. During this period, only on three days (21–23 January) the vortex was located above this region, so that the elevation of isentropes thinned the stratospheric ozone column, hence established an OMH-like situation. At the same time another OMH-like situation established over Western Siberia and moved eastward. Approximately over the Ural mountains, a fragmented low-PV area is found on 24 and 25 January 2011, indicative of a tropospheric ridge associated OMH condition. One day later, a PV streamer indicating a high tropopause started to establish east of the Mediterranean Sea, rapidly moving pole- and eastward, sliding below the vortex two days later on 27 January. For the next two days, until the 29th, the vortex was located above this relatively large region where the tropopause was elevated.

Between 24 and 26 January a broad band of very low temperatures connected the two regions exhibiting an elevated tropopause, approximately across the Siberian coast of the Arctic ocean. Even though the tropopause in this cold region was not distinctly elevated, the vortex-averaged temperature was low as 195 K between the tropopause and the 600 K isentrope over all days when ozone was low in both the GOME-2 total column and the limb vortex-average.

Although total ozone mapping from space inferred a rather coherent reduction of the ozone column during an elongated period in late January 2011, the meteorological situation clearly reveals that a superposition of two independently evolving synoptic events in the tropopause region formed two individual situations very similar to those causing ozone mini-holes. The two situations evolved from opposite sides of the Asian continent, both poleward of 60° N. We conclude that favourable meteorological condi-

tions in both the free troposphere and the lower stratosphere merged the two OMH-like situations after a few days of development, so that finally the thinning of ozone in the Arctic vortex appears like a single Arctic ozone mini-hole, covering large areas of the northern regions of Central Siberia.

3.8.2 Comparison to a typical OMH condition

The low ozone event in January 2011 is remarkable as it did not emerge over regions attributed to most frequent OMH occurrence. However, meteorological conditions responsible for this low ozone event were not different from these in the Northern Atlantic sector, where OMHs are found predominately. From the polar stereographic maps of near tropopause temperature and geopotential height (Figs. 13 and 14) one can infer a distinct and much larger ridge of tropospheric air (3 PV isoline), located over the North Atlantic on all days shown in the sequence. From the 26 January 2011 on it moved over the British Islands and Scandinavia, later reaching Central Europe. The tropopause there was distinctly elevated, substantially higher as in the regions where we identified the precursors of the low ozone “pocket” over Asia (Fig. 14). However, during the whole period, those tropopause ridges never slid under the vortex, which during the whole period was shifted towards Central Asia. Hence, tropopause elevations over the Northern Atlantic did not contribute to severe reductions in the stratospheric ozone column in late January 2011. In particular, they did not influence the ozone vortex-averages shown in Fig. 5.

Associated with this Scandinavian tropopause ridge a comparably small ozone mini-hole is seen in GOME-2 total ozone between 27 and 30 January 2011. In the relative coarse resolved CTM (resolution 2.5° in latitude, 3.75° in longitude) this OMH is not well reproduced. Only on 30 January 2011 the OMH is apparent in the CTM, a few degrees shifted to the northwest (Fig. 12).

The Arctic low ozone period 2011

R. Hommel et al.

Title Page

Abstract

Introduction

Conclusions

References

Tables

Figures

◀

▶

◀

▶

Back

Close

Full Screen / Esc

Printer-friendly Version

Interactive Discussion



3.8.3 Modelling the January 2011 Arctic low ozone event

As shown in Fig. 12, the CTM largely reproduces the day-to-day variability of stratospheric ozone over the Arctic. Only small-scale synoptic features like the Scandinavian ozone mini-hole around the 28 January 2011 are not adequately resolved. Also the magnitude of thinning the ozone column during the OMH-like situation is not captured well compared to GOME-2 observations. GOME-2 shows ozone as low as 200 DU on several days near the polar night blind spot, whereas the model's total ozone is not lower than 250 DU. Partly, this deficit is attributable to an approximated tropospheric contribution to the total ozone column.

A respective reduction in the height-resolved and vortex-averaged time-series of modelled Arctic ozone 2011 (Fig. 8) is not seen, in contrast to the vortex-average constructed from SCIAMACHY limb ozone profiles (Fig. 5). Although model data have been written at local times of SCIAMACHY overpasses and were sampled in similar manner as limb profiles in order to construct vortex-averages, i.e. grid cells lying within the vortex where modified PV > 38 PVU but south of 80° N, exhibiting SZAs < 88°, certain differences between the areas of the vortex covered by these two sampling methods persist. This may lead to the effect that in the model small-scale drops in the screened vortex O₃ mixing ratio are simply averaged out.

On the other hand, model equations are solved on isentropes. In the polar stratosphere isentropes are invariant to adiabatic processes in the tropopause region, so that a “thinning effect” in ozone mixing ratios above tropopause elevations is not apparent in the model vortex-average as long as the meridional divergence of ozone containing air out of the column is small. When the vortex-average is inferred from behaviour number densities, the “thinning effect” becomes apparent (not shown) and is in the order of 35 % below the 475 K isentrope, relative to average values in the undistorted vortex before and after this episode. This effect is approximately twice as large in the limb vortex-average (Sect. 3.3.2). Furthermore, in the model this “thinning effect” in the ozone number density does not extend well into the stratosphere. Projected on

Title Page

Abstract

Introduction

Conclusions

References

Tables

Figures

◀

▶

◀

▶

Back

Close

Full Screen / Esc

Printer-friendly Version

Interactive Discussion



The Arctic low ozone period 2011R. Hommel et al.

[Title Page](#)[Abstract](#)[Introduction](#)[Conclusions](#)[References](#)[Tables](#)[Figures](#)[◀](#)[▶](#)[◀](#)[▶](#)[Back](#)[Close](#)[Full Screen / Esc](#)[Printer-friendly Version](#)[Interactive Discussion](#)

geometric altitudes, this effect disappears at least 2 km below the regions in respective limb profiles. Whether meridional divergence of ozone containing air out of the column is underestimated in the CTM and better resolved in the vortex-average from limb measured ozone profiles, cannot be satisfactorily answered yet. However, such an underestimation is not unlikely because the model runs in a relatively coarse horizontal resolution so that numerical diffusion may play a role here even if the model's driving meteorology (ERA-Interim) is reproducing well the dynamical aspects of the OMH situation.

3.8.4 Implications for vortex-average ozone loss estimates

What do these conclusions mean for the vortex-average inferred from SCIAMACHY limb measurements and the model during time of the OMH-like situation in the Arctic stratosphere between 21 and 29 January 2011?

First, one has to also keep in mind that limb (as nadir) measurements depend on sunlight, so that during this specific period vortex regions north of 75° N were not observed. But between 21 and 30 January 2011 the vortex appeared not perfectly circumpolar, rather rotated off-centred from the geographic pole and was markedly displaced towards Siberia. This led to a situation, that a larger area of the vortex was illuminated by the sun, thus was observed, than if the vortex would have been shaped more perfectly circumpolar, rotating well-centred above the pole. As described above, the largest part of this sunlit area exhibited low ozone values. The few profiles from regions within the vortex showing larger, quasi undisturbed ozone values not being affected by tropopause elevations consequently do not contribute much to the daily mean vortex-averages. Hence, the transient lowering of ozone seen in the time-series of vortex-averaged limb ozone of Fig. 5 is reflecting a real situation.

However, the conversion of the retrieved number density profiles into mixing ratios on isentropic surfaces involves an error or bias through uncertainties in the gridded meteorological data sets used in this conversion. A few percent bias or uncertainty in temperature and pressure translates mainly into a vertical displacement of the pro-

The Arctic low ozone period 2011R. Hommel et al.

[Title Page](#)[Abstract](#)[Introduction](#)[Conclusions](#)[References](#)[Tables](#)[Figures](#)[◀](#)[▶](#)[◀](#)[▶](#)[Back](#)[Close](#)[Full Screen / Esc](#)[Printer-friendly Version](#)[Interactive Discussion](#)

jection from geometric altitudes to isentropes and to a lesser extent into a bias of the magnitude of the estimated “dynamical loss”. A 2 % deviation in the meteorology, for instance, yield vertical displacements of the limb vortex-mean mini-hole structure on the order of 10 K. But since the number density to mixing ratio conversion is proportional $\sim T/p$, a bias in coherent meteorological fields should almost have no effect.

From the time-series of the SCIAMACHY measured PSC occurrence rate (Fig. 9a) and OCIO at 90° SZA (Fig. 10a) as a proxy for chlorine activation, it is seen that the OMH-like situation in January 2011 had a direct impact on the chemical ozone destruction later in spring via the induced low temperatures in the stratosphere. These favoured PSC formation after the 24 of January 2011 and subsequently amplified chlorine activation.

It has to be mentioned that also the 2011 BrO vortex-average in Fig. 5 shows a “thinning effect” similar to that in ozone between 21 and 30 January 2011. This “thinning” extends well into the middle stratosphere close to the 575 K isentropic surface. Relative to values before and after the event, approximately 45 % less BrO is observed at 450 K and ~ 25 % at 550 K.

Of course, from such an investigation of a singular event we cannot claim that such dynamically induced phenomena are representative for the recent past nor that they are indicative of developments in a stratosphere impacted by climate change. But since those conditions are playing an important role in the chemistry of the polar stratosphere, an increase in their occurrence would substantially reinforcing ozone depletion even when the ozone layer recovers to values of the pre-CFC era.

4 Conclusions

Data products from the instruments SCIAMACHY and GOME/GOME-2 have been used in this study to investigate the state of ozone in Arctic winters from 2002/2003 to 2010/2011. As an example of the large year-to-year variation in Arctic ozone, the different behaviours of O₃ in the consecutive boreal winter–spring periods in 2009/2010

The Arctic low ozone period 2011R. Hommel et al.

[Title Page](#)[Abstract](#)[Introduction](#)[Conclusions](#)[References](#)[Tables](#)[Figures](#)[◀](#)[▶](#)[◀](#)[▶](#)[Back](#)[Close](#)[Full Screen / Esc](#)[Printer-friendly Version](#)[Interactive Discussion](#)

and 2010/2011 have been investigated in more detail. Height-resolved time-series of vortex-averaged O_3 , BrO, NO_2 from SCIAMACHY limb-scattering and solar occultation measurements were analyzed. From limb-scatter observations we infer chemically-induced ozone losses by employing the vortex-average technique described by Eichmann et al. (2002). SCIAMACHY observations of PSCs from the limb viewing geometry are used together with nadir OCIO slant columns at 90° SZA to further identify different behaviours of ozone depleting processes during the SCIAMACHY lifetime. Our understanding and ability to accurately simulate polar ozone depleting processes was tested with a three-dimensional isentropic chemistry transport model for the years 2010 and 2011.

From limb measurements, we infer ozone losses of more than 70 % below the 550 K isentropic surface in spring 2011, which corresponds well to estimates of previous studies (Manney et al., 2011; Sinnhuber et al., 2011; Arnone et al., 2012). In contrast, in spring 2010, when the vortex was much warmer and weaker than in 2011, chemically-induced ozone losses amount to only about 20 %. Differences in the vortex dynamics, coupled with the chemical processing of O_3 between the two winters and springs account for differences in the ozone time-series above the 550 K isentropic surface. In 2010, the variability in the O_3 profiles is quite large at the upper layers and about twice as much ozone is depleted via NO_x photochemistry than via heterogeneous processing on PSCs.

The O_3 vortex-average mixing ratios indicate another, previously unreported, loss feature in winter 2011 which occurred prior to the large chemical destruction of O_3 . For about ten days commencing 20 January 2011, column ozone over the Arctic decreased rapidly by more than 70 DU. Limb measurements show that below the 500 K isentrope ozone was reduced by up to 60 % to values as low as 1.5 ppmv. It turns out that a superposition of two independently evolving synoptic tropopause elevations over the Asian continent lowered the stratospheric ozone column by adiabatically lifting isentropes in the stratosphere – a situation which is commonly referred to as an “ozone mini-hole”. This involves a horizontal “redistribution” of ozone from the column

The Arctic low ozone period 2011R. Hommel et al.

[Title Page](#)[Abstract](#)[Introduction](#)[Conclusions](#)[References](#)[Tables](#)[Figures](#)[◀](#)[▶](#)[◀](#)[▶](#)[Back](#)[Close](#)[Full Screen / Esc](#)[Printer-friendly Version](#)[Interactive Discussion](#)

(horizontal divergence) which is better traced in the ozone profiles from SCIAMACHY limb than in the CTM. Due to the relatively coarse horizontal resolution the model does not adequately resolve this meridional dispersion of ozone out of the elevated column. Together with differences in the sampling of the data in the illuminated part of the vortex this leads to a different temporal development of the vortex-averaged time-series in the model compared to that inferred from limb profiles. The induced adiabatic cooling of the stratosphere during this period fostered further PSC formation so that more chlorine was activated in turn. It is not unlikely that the occurrence of this enlarged “ozone mini-hole”-like situation in mid-January 2011 may have substantially contributed that ozone destruction later in spring became as intense as observed. The region occupied an area almost as large as a chemically-induced ozone hole, that is at least a third larger than the area covered by “ozone mini-holes” typically.

In the strong and persistent Arctic vortex 2011 slightly lower levels of BrO were observed than 2010, which are accountable to a weaker meridional transport from tropical source regions during autumn and winter 2010/2011. Later in the two years, when the vortex became progressively unstable, vortex BrO decreased as NO₂ levels increased: the latter being attributed to increased horizontal mixing.

BrO and NO₂ are biased low in modelled Arctic vortices in both years. In other respects CTM simulations are generally in good agreement with the observations presented here. In particular the day-to-day variability of polar cap ozone and the large ozone losses from heterogenous processing in spring 2011 are represented well, though the latter is slightly overestimated.

In agreement with previous studies using other satellite instruments (e.g. Manney et al., 2011; Khosrawi et al., 2012) SCIAMACHY observations show that the season of PSC formation was prolonged in 2011 as never observed before over the Arctic. In this respect also chlorine activation was until then the strongest in the entire SCIAMACHY period.

In this manuscript we described correlative observations of the compositional state of the Arctic stratosphere during winter–spring 2010/2011, when the so far most se-

The Arctic low ozone period 2011R. Hommel et al.

[Title Page](#)[Abstract](#)[Introduction](#)[Conclusions](#)[References](#)[Tables](#)[Figures](#)[◀](#)[▶](#)[◀](#)[▶](#)[Back](#)[Close](#)[Full Screen / Esc](#)[Printer-friendly Version](#)[Interactive Discussion](#)

vere ozone losses have been reported. We compared the situation particularly with 2009/2010 as an example of a typical weak Arctic vortex exhibiting higher ozone levels. To understand the chemical composition of the Arctic stratosphere improves our knowledge about the processes determining the observed large intrinsic variability of Arctic ozone levels. This is of concern when assessing the predicability of future ozone and accompanied polar winter extremes because it is suspected that global climate change impacts stratospheric conditions. Although in general our CTM has been able to provide reasonable agreement with the observations, there are several detailed issues to be resolved in further work. Finally, the observation of a large OMH coupled to a large Northern Hemisphere polar ozone hole is not a coincidence. The issue is how often will such events occur in the future in a warming climate.

Acknowledgements. This work was funded by the European commission under the project “Stratospheric ozone: Halogen Impacts in a Varying Atmosphere” (SHIVA; FP7-ENV-2007-1-226224), the DFG Research Unit 1095 “Stratospheric Change and its Role for Climate Prediction” (SHARP) and was supported by the University of Bremen. CvS was partly supported by the University of Greifswald. Part of this work was supported by the project DACCS as part of the DFG priority program CAWSES. We thank several colleagues for suggestions and comments on the manuscript, in particular Hans F. Graf and Björn-Martin Sinnhuber, as well as Felix Ebojie, Katja Weigel, Stefan Noël, Claus Gebhardt and Emmanouil Proestakis. We also like to thank Gregor Kieseewetter, Peter Voelger, and Michael C. Pitts for providing access to additional data.

References

- Arnone, E., Castelli, E., Papandrea, E., Carlotti, M., and Dinelli, B. M.: Extreme ozone depletion in the 2010–2011 Arctic winter stratosphere as observed by MIPAS/ENVISAT using a 2-D tomographic approach, *Atmos. Chem. Phys.*, 12, 9149–9165, doi:10.5194/acp-12-9149-2012, 2012. 16616, 16625, 16634
- Aschmann, J., Sinnhuber, B.-M., Atlas, E. L., and Schauffler, S. M.: Modeling the transport of very short-lived substances into the tropical upper troposphere and lower stratosphere, *Atmos. Chem. Phys.*, 9, 9237–9247, doi:10.5194/acp-9-9237-2009, 2009. 16608

The Arctic low ozone period 2011R. Hommel et al.

[Title Page](#)[Abstract](#)[Introduction](#)[Conclusions](#)[References](#)[Tables](#)[Figures](#)[◀](#)[▶](#)[◀](#)[▶](#)[Back](#)[Close](#)[Full Screen / Esc](#)[Printer-friendly Version](#)[Interactive Discussion](#)

- Aschmann, J., Sinnhuber, B.-M., Chipperfield, M. P., and Hossaini, R.: Impact of deep convection and dehydration on bromine loading in the upper troposphere and lower stratosphere, *Atmos. Chem. Phys.*, 11, 2671–2687, doi:10.5194/acp-11-2671-2011, 2011. 16609, 16616
- 5 Balis, D., Isaksen, I. S. A., Zerefos, C., Zyrichidou, I., Eleftheratos, K., Tourpali, K., Bojkov, R., Rognerud, B., Stordal, F., Søvde, O. A., and Orsolini, Y.: Observed and modelled record ozone decline over the Arctic during winter/spring 2011, *Geophys. Res. Lett.*, 38, L23801, doi:10.1029/2011GL049259, 2011. 16625
- Bauer, R., Rozanov, A., McLinden, C. A., Gordley, L. L., Lotz, W., Russell III, J. M., Walker, K. A., Zawodny, J. M., Ladstätter-Weißenmayer, A., Bovensmann, H., and Burrows, J. P.: Validation of SCIAMACHY limb NO₂ profiles using solar occultation measurements, *Atmos. Meas. Tech.*, 5, 1059–1084, doi:10.5194/amt-5-1059-2012, 2012. 16603
- 10 Bovensmann, H., Burrows, J. P., Buchwitz, M., Frerick, J., Noël, S., Rozanov, V. V., Chance, K. V., and Goede, A. P. H.: Sciamachy: mission objectives and measurement modes, *J. Atmos. Sci.*, 56, 127–150, 1999. 16601, 16602
- 15 Bracher, A., Lamsal, L. N., Weber, M., Bramstedt, K., Coldewey-Egbers, M., and Burrows, J. P.: Global satellite validation of SCIAMACHY O₃ columns with GOME WFDOAS, *Atmos. Chem. Phys.*, 5, 2357–2368, doi:10.5194/acp-5-2357-2005, 2005. 16606
- Bramstedt, K., Amekudzi, L., Bracher, A., Rozanov, A., Bovensmann, H., and Burrows, J. P.: SCIAMACHY Solar Occultation: Ozone and NO₂ Profiles from 2002–2006, in: *Proceeding of the ERS-Envisat Symposium, ESA-SP 636, ESA Publications Division, 23–27 April 2007, Montreux, Switzerland, ISBN: 92-9291-200-1, 2007. 16604*
- 20 Bramstedt, K., Noël, S., Bovensmann, H., Gottwald, M., and Burrows, J. P.: Precise pointing knowledge for SCIAMACHY solar occultation measurements, *Atmos. Meas. Tech.*, 5, 2867–2880, doi:10.5194/amt-5-2867-2012, 2012. 16604
- 25 Burrows, J., Weber, M., Buchwitz, M., Rozanov, V. V., Ladstätter-Weißenmayer, A., Richter, A., DeBeek, R., Hoogen, R., Bramstedt, K., and Eichmann, K.: The Global Ozone Monitoring Experiment (GOME): mission concept and first scientific results, *J. Atmos. Sci.*, 56, 151–175, doi:10.1175/1520-0469(1999)056<0151:TGOMEG>2.0.CO;2, 1999. 16601, 16602
- Burrows, J. P., Platt, U., and Borrell, P.: *The Remote Sensing of Tropospheric Composition from Space, 1st Edn., Springer, Heidelberg, Germany, 2011. 16604*
- 30 Burrows, J. P., Hölzle, E., Goede, A., Visser, H., and Fricke, W.: SCIAMACHY – scanning imaging absorption spectrometer for atmospheric cartography, *Acta Astronaut.*, 35, 445–451, 1995. 16601, 16602

The Arctic low ozone period 2011R. Hommel et al.

[Title Page](#)[Abstract](#)[Introduction](#)[Conclusions](#)[References](#)[Tables](#)[Figures](#)[◀](#)[▶](#)[◀](#)[▶](#)[Back](#)[Close](#)[Full Screen / Esc](#)[Printer-friendly Version](#)[Interactive Discussion](#)

- Callies, J., Corpaccioli, E., Eisinger, M., Hahne, A., and Lefebvre, A.: GOME-2 – METOP's second-generation sensor for operational ozone monitoring, *ESA Bull.*, 102, 28–36, 2000. 16602
- Chipperfield, M. P.: Multiannual simulations with a three-dimensional chemical transport model, *J. Geophys. Res.*, 104, 1781–1805, 1999. 16609
- Coldewey-Egbers, M., Weber, M., Lamsal, L. N., de Beek, R., Buchwitz, M., and Burrows, J. P.: Total ozone retrieval from GOME UV spectral data using the weighting function DOAS approach, *Atmos. Chem. Phys.*, 5, 1015–1025, doi:10.5194/acp-5-1015-2005, 2005. 16606
- Dhomse, S., Weber, M., Wohltmann, I., Rex, M., and Burrows, J. P.: On the possible causes of recent increases in northern hemispheric total ozone from a statistical analysis of satellite data from 1979 to 2003, *Atmos. Chem. Phys.*, 6, 1165–1180, doi:10.5194/acp-6-1165-2006, 2006. 16599
- Doicu, A., Hilgers, S., von Bargaen, A., Rozanov, A., Eichmann, K.-U., von Savigny, C., and Burrows, J. P.: Information operator approach and iterative regularization methods for atmospheric remote sensing, *J. Quant. Spectrosc. Ra.*, 103, 340–350, doi:10.1016/j.jqsrt.2006.05.002, 2007. 16603
- Eichmann, K.-U., Weber, M., Bramstedt, K., and Burrows, J.: Ozone depletion in the NH winter/spring 1999/2000 as measured by GOME-ERS2, *J. Geophys. Res.*, 107, 8280, doi:10.1029/2001JD001148, 2002. 16600, 16607, 16613, 16615, 16625, 16634, 16650
- Feng, W., Chipperfield, M. P., Davies, S., von der Gathen, P., Kyrö, E., Volk, C. M., Ulanovsky, A., and Belyaev, G.: Large chemical ozone loss in 2004/2005 Arctic winter/spring, *Geophys. Res. Lett.*, 34, L09803, doi:10.1029/2006GL029098, 2007. 16623
- Fortuin, P. J. F. and Kelder, H.: An ozone climatology based on ozonesonde and satellite measurements, *J. Geophys. Res.*, 103, 31709–31734, doi:10.1029/1998JD200008, 1998. 16610, 16611, 16657
- Fusco, A. and Salby, M.: Interannual variations of total ozone and their relationship to variations of planetary wave activity, *J. Climate*, 12, 1619–1629, 1999. 16599
- Han, J., Yamazaki, K., and Niwano, M.: The winter ozone minimum over the subtropical northwestern Pacific, *J. Meteorol. Soc. Jpn.*, 81, 57–67, doi:10.2151/jmsj.83.57, 2005. 16627
- Hartmann, D. L., Wallace, J. M., Limpasuvan, V., Thompson, D. W. J., and Holton, J. R.: Can ozone depletion and global warming interact to produce rapid climate change?, *P. Natl. Acad. Sci. USA*, 97, 1412–1417, 2000. 16599

The Arctic low ozone period 2011

R. Hommel et al.

Title Page

Abstract

Introduction

Conclusions

References

Tables

Figures

◀

▶

◀

▶

Back

Close

Full Screen / Esc

Printer-friendly Version

Interactive Discussion



Hendrick, F., Van Roozendael, M., Kylling, A., Petritoli, A., Rozanov, A., Sanghavi, S., Schofield, R., von Friedeburg, C., Wagner, T., Wittrock, F., Fonteyn, D., and De Mazière, M.: Intercomparison exercise between different radiative transfer models used for the interpretation of ground-based zenith-sky and multi-axis DOAS observations, *Atmos. Chem. Phys.*, 6, 93–108, doi:10.5194/acp-6-93-2006, 2006. 16605

Hoogen, R., Rozanov, V. V., and Burrows, J. P.: Ozone profiles from GOME satellite data: algorithm description and first validation, *J. Geophys. Res.*, 104, 8263–8280, doi:10.1029/1998JD100093, 1999. 16603

Hurwitz, M. M., Newman, P. A., and Garfinkel, C. I.: The Arctic vortex in March 2011: a dynamical perspective, *Atmos. Chem. Phys.*, 11, 11447–11453, doi:10.5194/acp-11-11447-2011, 2011. 16599, 16625

James, P. M.: An interhemispheric comparison of ozone mini-hole climatologies, *Geophys. Res. Lett.*, 25, 301–304, 1998. 16626, 16627

JPL/NASA: Chemical Kinetics and Photochemical Data for Use in Atmospheric Studies, JPL Publication 06-2, Evaluation No 15, edited by: Sander, S. P., Friedl, R. R., Ravishankara, A. R., Golden, D. M., Kolb, C. E., Kurylo, M. J., Huie, R. E., Orkin, V. L., Molina, M. J., Moortgat, G. K., and Finlayson-Pitts, B. J., NASA Jet Propulsion Laboratory, California Institute of Technology, Pasadena, California, 2006. 16609

Khosrawi, F., Urban, J., Pitts, M. C., Voelger, P., Achtert, P., Kaphlanov, M., Santee, M. L., Manney, G. L., Murtagh, D., and Fricke, K.-H.: Denitrification and polar stratospheric cloud formation during the Arctic winter 2009/2010, *Atmos. Chem. Phys.*, 11, 8471–8487, doi:10.5194/acp-11-8471-2011, 2011. 16600, 16621, 16622, 16624

Khosrawi, F., Urban, J., Pitts, M. C., Voelger, P., Achtert, P., Santee, M. L., Manney, G. L., and Murtagh, D. (Eds.): Denitrification and polar stratospheric cloud formation during the Arctic winter 2009/2010 and 2010/2011 in comparison, *Proceedings of the ESA Atmospheric Science Conference 18–22 June 2012, Bruges, Belgium, ESA-SP-708, Eur. Space Agency Spec. Publ.*, November 2012, ISBN/ISSN:978-92-9092-272-8, 2012. 16614, 16621, 16622, 16635

Kiesewetter, G., Sinnhuber, B.-M., Vountas, M., Weber, M., and Burrows, J. P.: A long-term stratospheric ozone data set from assimilation of satellite observations: high-latitude ozone anomalies, *J. Geophys. Res.*, 115, D10307, doi:10.1029/2009JD013362, 2010a. 16607

The Arctic low ozone period 2011

R. Hommel et al.

[Title Page](#)[Abstract](#)[Introduction](#)[Conclusions](#)[References](#)[Tables](#)[Figures](#)[◀](#)[▶](#)[◀](#)[▶](#)[Back](#)[Close](#)[Full Screen / Esc](#)[Printer-friendly Version](#)[Interactive Discussion](#)

- Kiesewetter, G., Sinnhuber, B.-M., Weber, M., and Burrows, J. P.: Attribution of stratospheric ozone trends to chemistry and transport: a modelling study, *Atmos. Chem. Phys.*, 10, 12073–12089, doi:10.5194/acp-10-12073-2010, 2010b. 16607, 16609
- 5 Koch, G., Wernli, H., Schwierz, C., Staehelin, J., and Peter, T.: A composite study on the structure and formation of ozone miniholes and minihighs over central Europe, *Geophys. Res. Lett.*, 32, L12810, doi:10.1029/2004GL022062, 2005. 16627, 16628
- Konopka, P., Engel, A., Funke, B., Müller, R., Grooß, J.-U., Günther, G., Wetter, T., Stiller, G., von Clarmann, T., Glatthor, N., Oelhaf, H., Wetzela, G., López-Puertas, M., Pirre, M., Huret, N., and Riese, M.: Ozone loss driven by nitrogen oxides and triggered by stratospheric warmings can outweigh the effect of halogens, *J. Geophys. Res.*, 112, D5105, doi:10.1029/2006JD007064, 2007. 16614, 16615
- 10 Kozlov, V.: Design of experiments related to the inverse of mathematical physics, in: *Mathematical Theory of Experiment Design*, edited by: Ermakov, C. M., Nauka, Moscow, 216–246, 1983 (in Russian). 16603
- 15 Krzyścin, J. W.: Long-term changes in ozone mini-hole event frequency over the Northern Hemisphere derived from ground-based measurements, *Int. J. Climatol.*, 22, 1425–1439, doi:10.1002/joc.812, 2002. 16627, 16628
- Lary, D. J., Chipperfield, M. P., Toumi, R., and Lenton, T.: Heterogeneous atmospheric bromine chemistry, *J. Geophys. Res.*, 101, 1489–1504, doi:10.1029/95JD02839, 1996. 16617
- 20 Liu, C., Liu, Y., Cai, Z., Gao, S., Lü, D., and Kyrölä, E.: A Madden–Julian Oscillation-triggered record ozone minimum over the Tibetan Plateau in December 2003 and its association with stratospheric “low-ozone pockets”, *Geophys. Res. Lett.*, 36, L15830, doi:10.1029/2009GL039025, 2009. 16627
- Mäder, J. A., Staehelin, J., Peter, T., Brunner, D., Rieder, H. E., and Stahel, W. A.: Evidence for the effectiveness of the Montreal Protocol to protect the ozone layer, *Atmos. Chem. Phys.*, 10, 12161–12171, doi:10.5194/acp-10-12161-2010, 2010. 16600
- 25 Manney, G. L., Santee, M. L., Froidevaux, L., Hoppel, K., Livesey, N. J., and Waters, J. W.: EOS MLS observations of ozone loss in the 2004–2005 Arctic winter, *Geophys. Res. Lett.*, 33, L04802, doi:10.1029/2005GL024494, 2006. 16623
- 30 Manney, G. L., Santee, M. L., Rex, M., Livsey, N. J., Pitts, M. C., Veefkind, P., Nash, E. R., Wohltmann, I., Lehmann, R., Froidevaux, L., Poole, L. R., Schoeberl, M. R., Haffner, D. P., Davies, J., Dorokhov, V., Gernandt, H., Johnson, B., Kivi, R., Kyrö, E., Larsen, N., Levelt, P. F., Makshtas, A., McElroy, C. T., Nakajima, H., Parrondo, M. C., Tarasick, D. W., von der Ga-

The Arctic low ozone period 2011

R. Hommel et al.

[Title Page](#)[Abstract](#)[Introduction](#)[Conclusions](#)[References](#)[Tables](#)[Figures](#)[◀](#)[▶](#)[◀](#)[▶](#)[Back](#)[Close](#)[Full Screen / Esc](#)[Printer-friendly Version](#)[Interactive Discussion](#)

then, P., Walker, K. A., and Zinoviev, N. S.: Unprecedented Arctic ozone loss in 2011, *Nature*, 478, 469–475, doi:10.1038/nature10556, 2011. 16599, 16600, 16611, 16614, 16615, 16616, 16622, 16623, 16624, 16625, 16634, 16635

5 McLinden, C. A., Olsen, S. C., Hannegan, B., Wild, O., Prather, M. J., and Sundet, J.: Stratospheric ozone in 3-D models: a simple chemistry and the cross-tropopause flux, *J. Geophys. Res.*, 105, 14653–14665, doi:10.1029/2000JD900124, 2000. 16609

10 McLinden, C. A., Haley, C. S., Lloyd, N. D., Hendrick, F., Rozanov, A., Sinnhuber, B., Goutail, F., Degenstein, D. A., Llewellyn, E. J., Sioris, C. E., Van Roozendael, M., Pomereau, J. P., Lotz, W., and Burrows, J. P.: Odin/OSIRIS observations of stratospheric BrO: retrieval methodology, climatology, and inferred Bry, *J. Geophys. Res.*, 115, D15308, doi:10.1029/2009JD012488, 2010. 16614

Meyer, J., Bracher, A., Rozanov, A., Schlesier, A. C., Bovensmann, H., and Burrows, J. P.: Solar occultation with SCIAMACHY: algorithm description and first validation, *Atmos. Chem. Phys.*, 5, 1589–1604, doi:10.5194/acp-5-1589-2005, 2005. 16604

15 Mieruch, S., Weber, M., von Savigny, C., Rozanov, A., Bovensmann, H., Burrows, J. P., Bernath, P. F., Boone, C. D., Froidevaux, L., Gordley, L. L., Mlynczak, M. G., Russell III, J. M., Thomason, L. W., Walker, K. A., and Zawodny, J. M.: Global and long-term comparison of SCIAMACHY limb ozone profiles with correlative satellite data (2002–2008), *Atmos. Meas. Tech.*, 5, 771–788, doi:10.5194/amt-5-771-2012, 2012. 16603

20 Mitchell, D. M., Gray, L. J., and Charlton-Perez, A. J.: The structure and evolution of the stratospheric vortex in response to natural forcings, *J. Geophys. Res.*, 116, D15110, doi:10.1029/2011JD015788, 2011. 16599

Newman, P. A., Lait, L. R., and Schoeberl, M. R.: The morphology and meteorology of Southern Hemisphere spring total ozone mini-holes, *Geophys. Res. Lett.*, 15, 923–926, 1988. 16626, 16628

25 Noxon, J. F.: Stratospheric NO₂ 2: global behavior, *J. Geophys. Res.*, 84, 5067–5076, 1979. 16619

Oetjen, H., Wittrock, F., Richter, A., Chipperfield, M., Medeke, T., Sheode, N., Sinnhuber, B.-M., Sinnhuber, M., and Burrows, J. P.: Evaluation of stratospheric chlorine chemistry for the Arctic spring 2005 using modelled and measured OCIO column densities, *Atmos. Chem. Phys.*, 11, 689–703, doi:10.5194/acp-11-689-2011, 2011. 16605, 16606

30

The Arctic low ozone period 2011

R. Hommel et al.

[Title Page](#)[Abstract](#)[Introduction](#)[Conclusions](#)[References](#)[Tables](#)[Figures](#)[◀](#)[▶](#)[◀](#)[▶](#)[Back](#)[Close](#)[Full Screen / Esc](#)[Printer-friendly Version](#)[Interactive Discussion](#)

- Orsolini, Y. J., Stephenson, D. B., and Doblus-Reyes, F. J.: Storm track signature in total ozone during Northern Hemisphere winter, *Geophys. Res. Lett.*, 25, 2413, doi:10.1029/98GL01852, 1998. 16627
- Osterman, G. B., Salawitch, R. J., Sen, B., Toon, G. C., Stachnik, R. A., Pickett, H. M., Margitan, J. J., Blavier, J., and Peterson, D. B.: Balloon-borne measurements of stratospheric radicals and their precursors: implications for the production and loss of ozone, *Geophys. Res. Lett.*, 24, 1107–1110, doi:10.1029/97GL00921, 1997. 16615
- Pitts, M. C., Poole, L. R., Dörnbrack, A., and Thomason, L. W.: The 2009–2010 Arctic polar stratospheric cloud season: a CALIPSO perspective, *Atmos. Chem. Phys.*, 11, 2161–2177, doi:10.5194/acp-11-2161-2011, 2011. 16621
- Platt, U.: Differential optical absorption spectroscopy (DOAS), in: *Air Monitoring by Spectroscopic Techniques*, Chemical Analysis Series, edited by: Sigrist, M. W., John Wiley, New York, 127 pp., 1994. 16604, 16606
- Reed, R.: On the role of vertical motions in ozone-weather relationships, *J. Meteorol.*, 7, 263–267, 1950. 16626
- Rex, M., Salawitch, R. J., von der Gathen, P., Harris, N. R. P., Chipperfield, M. P., and Naujokat, B.: Arctic ozone loss and climate change, *Geophys. Res. Lett.*, 31, L04116, doi:10.1029/2003GL018844, 2004. 16600
- Richter, A., Wittrock, F., Weber, M., Beirle, S., Kühl, S., Platt, U., Wagner, T., Wilms-Grabe, W., and Burrows, J. P.: GOME observations of stratospheric trace gas distributions during the splitting vortex event in the Antarctic winter 2002 Part I: Measurements, *J. Atmos. Sci.*, 62, 778–785, 2005. 16604, 16605, 16610
- Rodgers, C. D.: *Inverse Methods for Atmospheric Sounding: Theory and Practice*, World Scientific, Singapore, 2000. 16603
- Rohen, G. J., Savigny, C. v., Kaiser, J. W., Llewellyn, E. J., Froidevaux, L., López-Puertas, M., Steck, T., Palm, M., Winkler, H., Sinnhuber, M., Bovensmann, H., and Burrows, J. P.: Ozone profile retrieval from limb scatter measurements in the HARTLEY bands: further retrieval details and profile comparisons, *Atmos. Chem. Phys.*, 8, 2509–2517, doi:10.5194/acp-8-2509-2008, 2008. 16603
- Rosenfield, J. E., Newman, P. E., and Schoeberl, M. R.: Computations of diabatic descent in the stratospheric polar vortex, *J. Geophys. Res.*, 99, 16677–16689, doi:10.1029/94JD01156, 1994. 16613, 16615

The Arctic low ozone period 2011

R. Hommel et al.

[Title Page](#)[Abstract](#)[Introduction](#)[Conclusions](#)[References](#)[Tables](#)[Figures](#)[◀](#)[▶](#)[◀](#)[▶](#)[Back](#)[Close](#)[Full Screen / Esc](#)[Printer-friendly Version](#)[Interactive Discussion](#)

- Rozanov, A., Bovensmann, H., Bracher, A., Hrechanyy, S., Rozanov, V., Sinnhuber, M., Stroh, F., and Burrows, J.: NO₂ and BrO vertical profile retrieval from SCIAMACHY limb measurements: Sensitivity studies, *Adv. Space Res.*, 36, 846–854, doi:10.1016/j.asr.2005.03.013, 2005. 16603
- 5 Rozanov, A., Kühl, S., Doicu, A., McLinden, C., Puķīte, J., Bovensmann, H., Burrows, J. P., Deutschmann, T., Dorf, M., Goutail, F., Grunow, K., Hendrick, F., von Hobe, M., Hrechanyy, S., Lichtenberg, G., Pfeilsticker, K., Pommereau, J. P., Van Roozendael, M., Stroh, F., and Wagner, T.: BrO vertical distributions from SCIAMACHY limb measurements: comparison of algorithms and retrieval results, *Atmos. Meas. Tech.*, 4, 1319–1359, doi:10.5194/amt-4-1319-2011, 2011a. 16603
- 10 Rozanov, A., Weigel, K., Bovensmann, H., Dhomse, S., Eichmann, K.-U., Kivi, R., Rozanov, V., Vömel, H., Weber, M., and Burrows, J. P.: Retrieval of water vapor vertical distributions in the upper troposphere and the lower stratosphere from SCIAMACHY limb measurements, *Atmos. Meas. Tech.*, 4, 933–954, doi:10.5194/amt-4-933-2011, 2011b. 16603
- 15 Salby, M., Titova, E., and Deschamps, L.: Rebound of Antarctic ozone, *Geophys. Res. Lett.*, 38, L09702, doi:10.1029/2011GL047266, 2011. 16600
- Shine, K. P.: The middle atmosphere in the absence of dynamic heat fluxes, *Q. J. Roy. Meteorol. Soc.*, 113, 603–633, 1987. 16609
- 20 Singleton, C., Randall, C., Harvey, V., Chipperfield, M., Feng, W., Manney, G., Froidevaux, L., Boone, C., Bernath, P., Walker, K., McElroy, C., and Hoppel, K.: Quantifying Arctic ozone loss during the 2004–2005 winter using satellite observations and a chemical transport model, *J. Geophys. Res.*, 112, D07304, doi:10.1029/2006JD007463, 2007. 16620
- Sinnhuber, B.-M., Arlander, D. W., Bovensmann, H., Burrows, J. P., Chipperfield, M. P., Enell, C.-F., Frieß, U., Hendrick, F., Johnston, P. V., Jones, R. L., Kreher, K., Mohamed-Tahrin, N., Müller, R., Pfeilsticker, K., Platt, U., Pommereau, J.-P., Pundt, I., Richter, A., South, A. M., Tørnkvist, K. K., Van Roozendael, M., Wagner, T., and Wittrock, F.: Comparison of measurements and model calculations of stratospheric bromine monoxide, *J. Geophys. Res.*, 107, 4398, doi:10.1029/2001JD000940, 2002. 16613
- 25 Sinnhuber, B.-M., Weber, M., Amankwah, A., and Burrows, J. P.: Total ozone during the unusual Antarctic winter of 2002, *Geophys. Res. Lett.*, 30, 1580, doi:10.1029/2002GL016798, 2003. 16608, 16609, 16616
- 30

The Arctic low ozone period 2011

R. Hommel et al.

Title Page

Abstract

Introduction

Conclusions

References

Tables

Figures

◀

▶

◀

▶

Back

Close

Full Screen / Esc

Printer-friendly Version

Interactive Discussion



- Sinnhuber, B.-M., Stiller, G., Ruhnke, R., von Clarmann, T., Kellmann, S., and Aschmann, J.: Arctic winter 2010/2011 at the brink of an ozone hole, *Geophys. Res. Lett.*, 38, L24814, doi:10.1029/2011GL049784, 2011. 16599, 16616, 16625, 16634
- 5 Sonkaew, T., Rozanov, V. V., von Savigny, C., Rozanov, A., Bovensmann, H., and Burrows, J. P.: Cloud sensitivity studies for stratospheric and lower mesospheric ozone profile retrievals from measurements of limb-scattered solar radiation, *Atmos. Meas. Tech.*, 2, 653–678, doi:10.5194/amt-2-653-2009, 2009. 16603
- 10 Sonkaew, T., von Savigny, C., Eichmann, K.-U., Weber, M., Rozanov, A., Bovensmann, H., Burrows, J. P., and Grooß, J.-U.: Chemical ozone losses in Arctic and Antarctic polar winter/spring season derived from SCIAMACHY limb measurements 2002–2009, *Atmos. Chem. Phys.*, 13, 1809–1835, doi:10.5194/acp-13-1809-2013, 2013. 16600, 16607, 16613, 16615, 16621, 16623
- 15 Steinbrecht, W., Köhler, U., Claude, H., Weber, M., Burrows, J. P., and van der A, R. J.: Very high ozone columns at northern mid-latitudes in 2010, *Geophys. Res. Lett.*, 38, L06803, doi:10.1029/2010GL046634, 2011. 16600, 16611
- Stolarski, R. S. and Frith, S. M.: Search for evidence of trend slow-down in the long-term TOMS/SBUV total ozone data record: the importance of instrument drift uncertainty, *Atmos. Chem. Phys.*, 6, 4057–4065, doi:10.5194/acp-6-4057-2006, 2006. 16607
- 20 Strahan, S. E., Douglass, A. R., and Newman, P. A.: The contributions of chemistry and transport to low arctic ozone in March 2011 derived from Aura MLS observations, *J. Geophys. Res.*, 118, 1563–1576, doi:10.1002/jgrd.50181, 2013. 16622
- Theys, N., Van Roozendael, M., Errera, Q., Hendrick, F., Daerden, F., Chabrillat, S., Dorf, M., Pfeilsticker, K., Rozanov, A., Lotz, W., Burrows, J. P., Lambert, J.-C., Goutail, F., Roscoe, H. K., and De Mazière, M.: A global stratospheric bromine monoxide climatology based on the BASCOE chemical transport model, *Atmos. Chem. Phys.*, 9, 831–848, doi:10.5194/acp-9-831-2009, 2009. 16614
- 25 von Savigny, C., Ulasi, E. P., Eichmann, K.-U., Bovensmann, H., and Burrows, J. P.: Detection and mapping of polar stratospheric clouds using limb scattering observations, *Atmos. Chem. Phys.*, 5, 3071–3079, doi:10.5194/acp-5-3071-2005, 2005a. 16605, 16606, 16622
- 30 von Savigny, C., Rozanov, A., Bovensmann, H., Eichmann, K.-U., Noël, S., Rozanov, V. V., Sinnhuber, B.-M., Weber, M., and Burrows, J. P.: The ozone hole break-up in September 2002 as seen by SCIAMACHY on ENVISAT, *J. Atmos. Sci.*, 62, 721–734, 2005b. 16605, 16610

The Arctic low ozone period 2011

R. Hommel et al.

Title Page

Abstract

Introduction

Conclusions

References

Tables

Figures

◀

▶

◀

▶

Back

Close

Full Screen / Esc

Printer-friendly Version

Interactive Discussion



Wagner, T., Wittrock, F., Richter, A., Wenig, M., Burrows, J. P., and Platt, U.: Continuous monitoring of the high and persistent chlorine activation during the Arctic winter 1999/2000 by the GOME instrument on ERS-2, *J. Geophys. Res.*, 107, 8267, doi:10.1029/2001JD000466, 2002. 16605

5 Weber, M., Eichmann, K.-U., Wittrock, F., Bramstedt, K., Hild, L., Richter, A., Burrows, J., and Müller, R.: The cold Arctic winter 1995/96 as observed by GOME and HALOE: tropospheric wave activity and chemical ozone loss, *Q. J. Roy. Meteorol. Soc.*, 128, 1293–1319, 2002. 16615, 16626, 16627

10 Weber, M., Lamsal, L. N., Coldewey-Egbers, M., Bramstedt, K., and Burrows, J. P.: Pole-to-pole validation of GOME WFDOAS total ozone with groundbased data, *Atmos. Chem. Phys.*, 5, 1341–1355, doi:10.5194/acp-5-1341-2005, 2005. 16606

15 Weber, M., Lamsal, L. N., and Burrows, J. P.: Improved SCIAMACHY WFDOAS total ozone retrieval: steps towards homogenising long-term total ozone datasets from GOME, SCIAMACHY, and GOME2, in: Proc. “Envisat Symposium 2007”, Montreux, Switzerland, 23–27 April 2007, ESA SP-636, July 2007, available at: <http://envisat.esa.int/envisatsymposium/proceedings/posters/3P4/463281we.pdf> (last access: 17 June 2013), 2007. 16606

20 Weber, M., Dikty, S., Burrows, J. P., Garny, H., Dameris, M., Kubin, A., Abalichin, J., and Langematz, U.: The Brewer-Dobson circulation and total ozone from seasonal to decadal time scales, *Atmos. Chem. Phys.*, 11, 11221–11235, doi:10.5194/acp-11-11221-2011, 2011. 16599, 16610, 16648

Winkler, H., Sinnhuber, M., Notholt, J., Kallenrode, M.-B., Steinhilber, F., Vogt, J., Zieger, B., Glassmeier, K.-H., and Stadelmann, A.: Modeling impacts of geomagnetic field variations on middle atmospheric ozone responses to solar proton events on long timescales, *J. Geophys. Res.*, 113, D02302, doi:10.1029/2007JD008574, 2008. 16609

25 WMO: Scientific Assessment of Ozone Depletion: 2010, Global Ozone Research and Monitoring Project, Report No. 52, World Meteorological Organization, Geneva, Switzerland, 2010. 16599, 16600, 16613

The Arctic low ozone period 2011

R. Hommel et al.

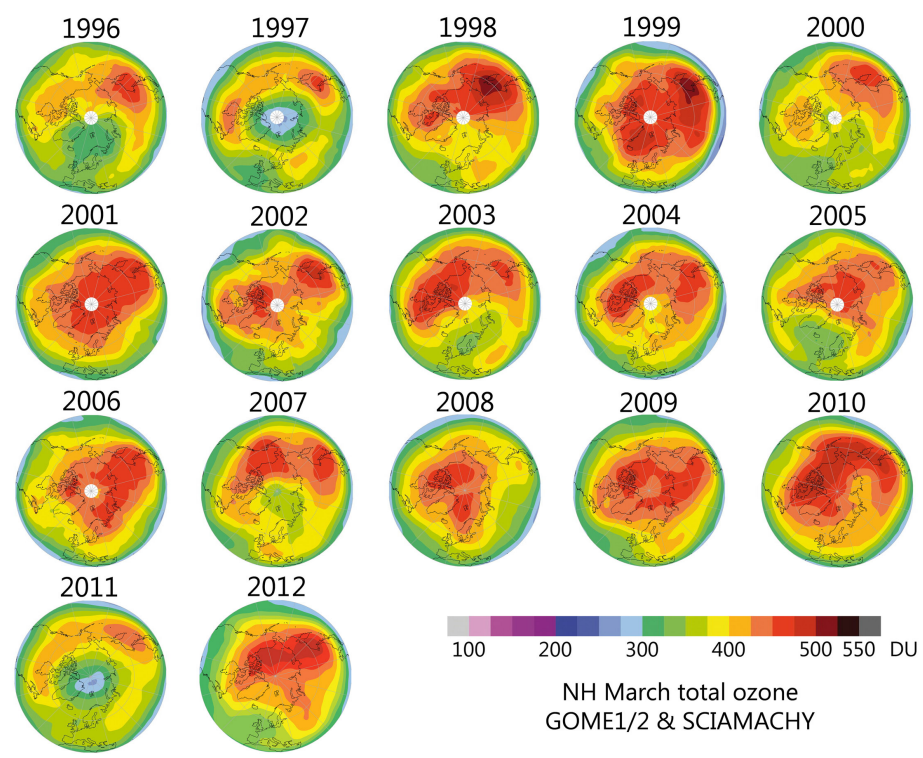


Fig. 1. Polar stereographic maps of March mean Arctic total ozone as obtained from the GSG data set, containing observations from GOME (1996–2003), SCIAMACHY (2003–2006) and GOME-2 (2007–2012).

Title Page	
Abstract	Introduction
Conclusions	References
Tables	Figures
◀	▶
◀	▶
Back	Close
Full Screen / Esc	
Printer-friendly Version	
Interactive Discussion	



The Arctic low ozone period 2011

R. Hommel et al.

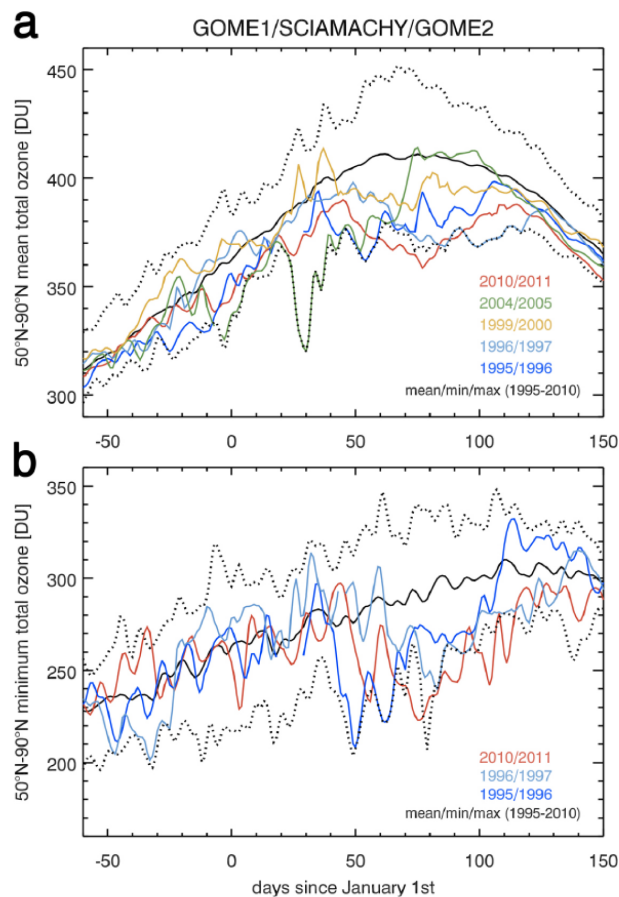


Fig. 2. Evolution of Arctic total ozone in the GSG data set for various cold winters with severe ozone losses since 1995. **(a)** Shows the area weighted mean and **(b)** the minimum total ozone as obtained from the GSG data set north of 50° N. Each time-series is also confined by respective mean, minimum and maximum values of the 16 yr data record 1995–2010.

The Arctic low ozone period 2011

R. Hommel et al.

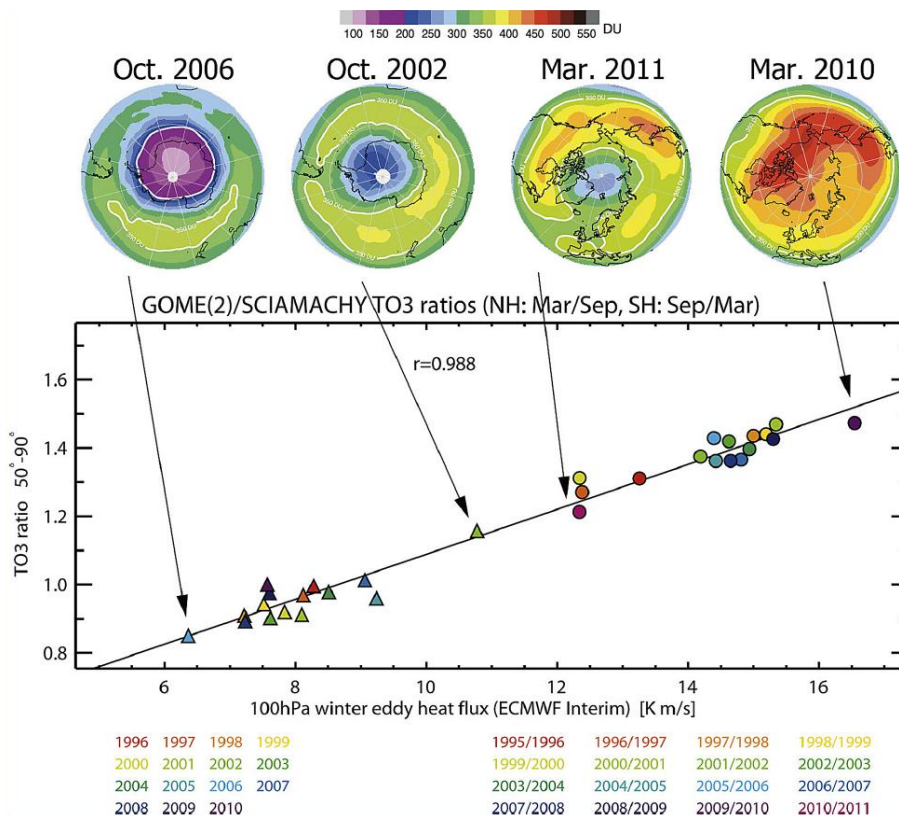


Fig. 3. Correlation between winter eddy heat flux and spring-to-fall ozone ratio over the polar caps (update from Weber et al., 2011). Triangles are data from the SH; circles from the NH.

Title Page

Abstract Introduction

Conclusions References

Tables Figures

◀ ▶

◀ ▶

Back Close

Full Screen / Esc

Printer-friendly Version

Interactive Discussion



The Arctic low ozone period 2011

R. Hommel et al.

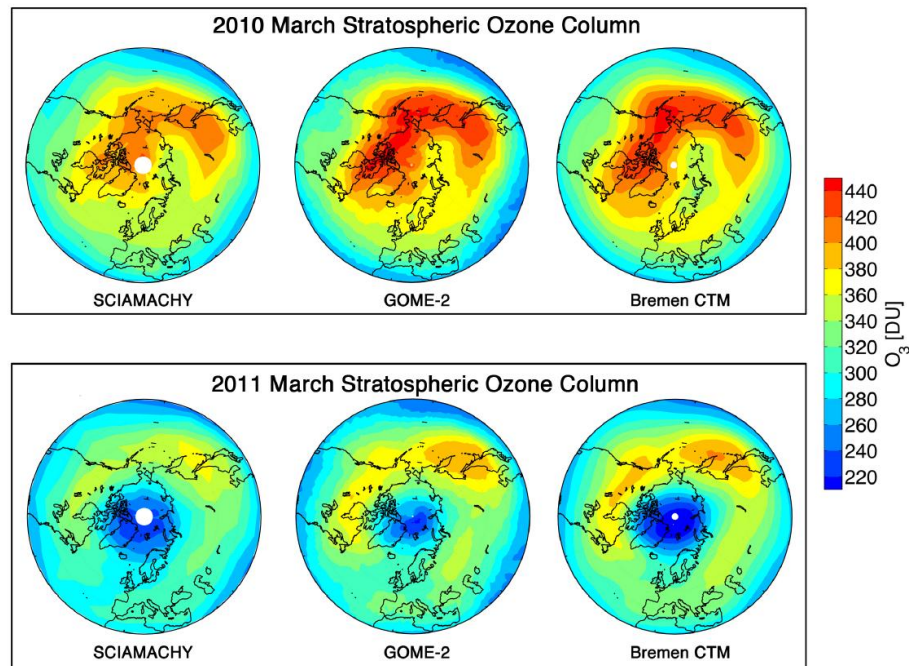


Fig. 4. March mean stratospheric columns of ozone in 2010 (top) and 2011 (bottom) as obtained from SCIAMACHY in limb viewing geometry (left), the nadir-viewing scanning spectrometer GOME-2 and as inferred from chemistry transport model calculations (right). For GOME-2 the stratospheric column was obtained by subtracting tropospheric ozone (climatological values) from the measured total ozone.

Winter-Spring SCIAMACHY Limb Vortex Averaged VMR

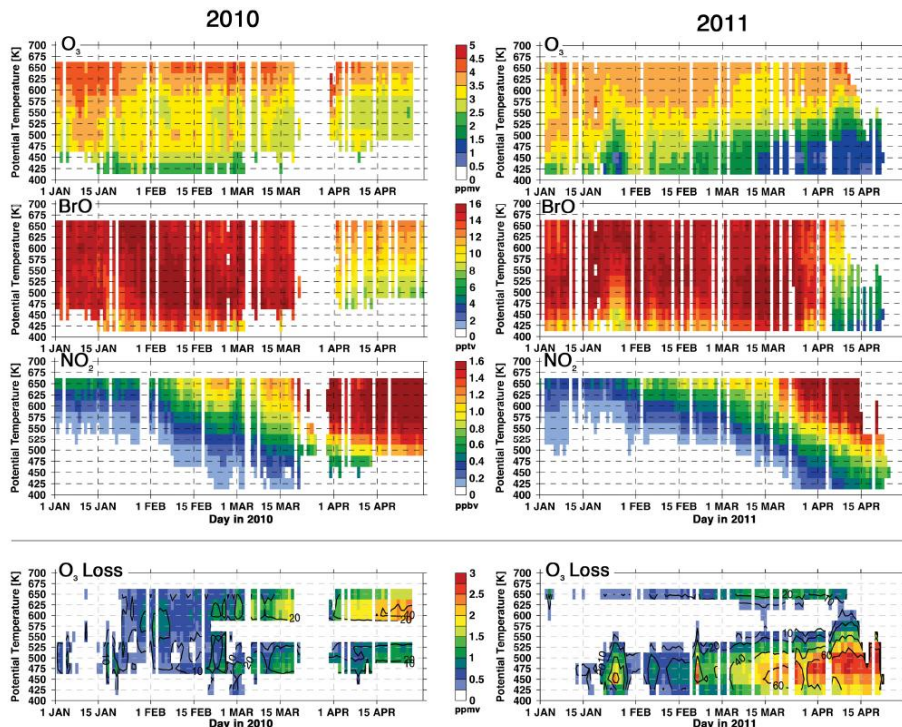


Fig. 5. Evolution of O_3 , BrO and NO_2 in the lower stratospheric Arctic polar vortex during the first four months of 2010 (left column) and 2011 (right column) as obtained from SCIAMACHY limb observations. Bottom panels show corresponding chemical ozone losses obtained by the method of Eichmann et al. (2002). Only those SCIAMACHY limb profiles are taken into account, where the modified potential vorticity (UKMO) exceeds 38 MPVU and the solar zenith angle is between 75° and 88° . Volume mixing ratios are colour shaded, black contour lines in the bottom panels denote relative ozone losses in %.

2011 Winter-Spring SCIAMACHY Occultation VMR Inside Vortex

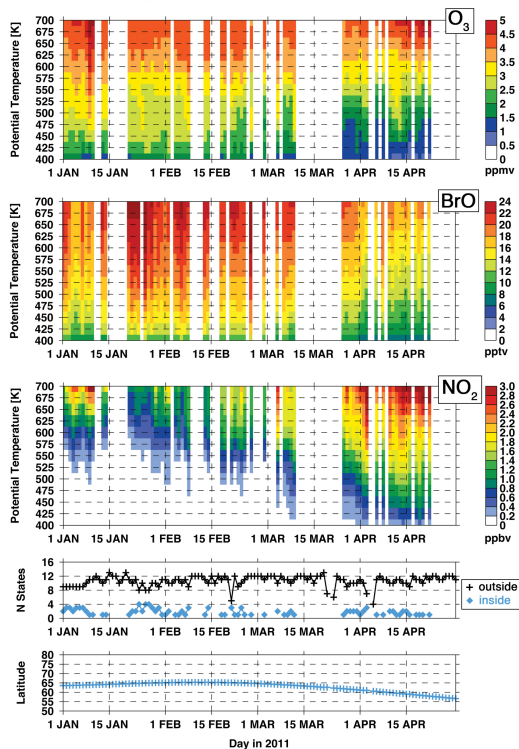


Fig. 6. Evolution of O_3 , BrO and NO_2 in the lower stratospheric Arctic polar vortex from 1 January 2011 to 30 April 2011 obtained from SCIAMACHY solar occultation observations. Only measurements within the polar vortex (modified potential vorticity > 38 PVU) are considered. The number of respective occultation measurements inside and outside the vortex, as well as the latitude of measurement, are shown in the bottom panels. Note the different plotting range of BrO and NO_2 compared to limb and model vortex-averages (Figs. 5 and 8).

The Arctic low ozone period 2011

R. Hommel et al.

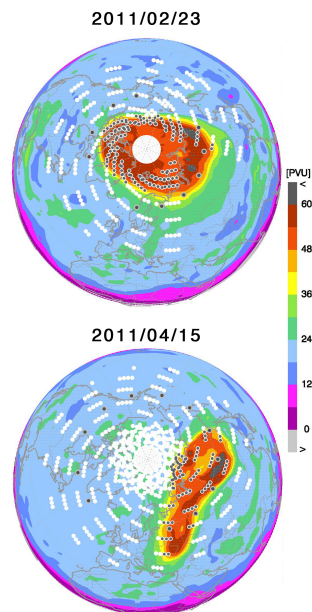


Fig. 7. Polar stereographic projection of the UKMO potential vorticity at the 475 K isentropic level. It also depicts the location of SCIAMACHY limb measurements (small dots) in comparison to SCIAMACHY solar occultation measurements (large dots), relative to the location and shape of the polar vortex at two days in winter–spring 2011 at 475 K. The edge of the polar vortex is at approximately 38 PVU modified potential vorticity. On 23 February (top), around the onset of the chemical ozone depletion the vortex had an almost circumpolar shape whereas on 15 April 2011 (bottom) it was highly distorted and shifted towards the Eurasian continent. Limb measurements lying within the vortex are shaded dark grey, locations outside are shaded white.

[Title Page](#)[Abstract](#)[Introduction](#)[Conclusions](#)[References](#)[Tables](#)[Figures](#)[◀](#)[▶](#)[◀](#)[▶](#)[Back](#)[Close](#)[Full Screen / Esc](#)[Printer-friendly Version](#)[Interactive Discussion](#)

The Arctic low ozone period 2011

R. Hommel et al.

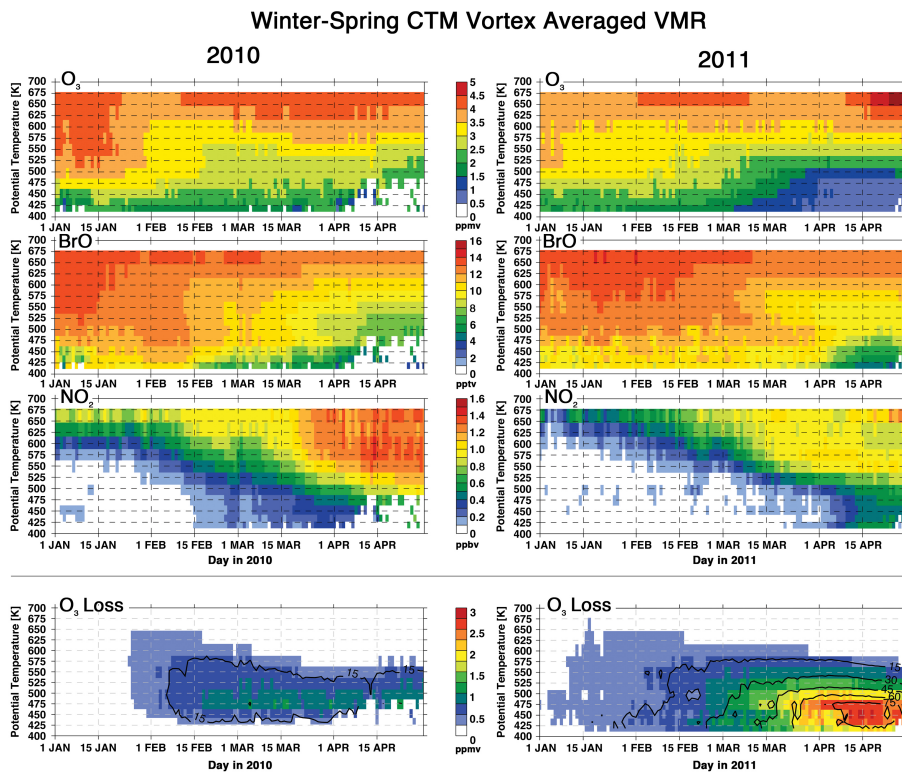


Fig. 8. As in Fig. 5, except for respective CTM simulations. Here, relative ozone losses are interpreted relative to the volume mixing ratio of a quasi-passive ozone tracer which is only affected by large-scale photochemistry, not considering heterogeneous reactions.

Title Page

Abstract Introduction

Conclusions References

Tables Figures

◀ ▶

◀ ▶

Back Close

Full Screen / Esc

Printer-friendly Version

Interactive Discussion



The Arctic low ozone period 2011

R. Hommel et al.

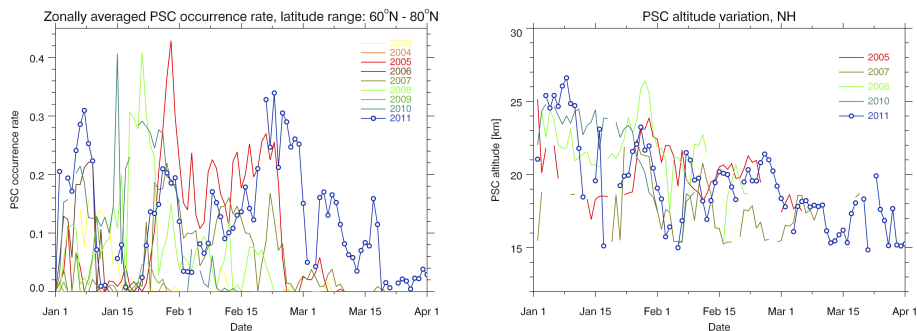


Fig. 9. PSC occurrence rate (a) and PSC altitude (b) obtained from SCIAMACHY limb observations since 2003. For clarity reasons only years with frequent PSC occurrences are displayed in the right panel.

[Title Page](#)[Abstract](#)[Introduction](#)[Conclusions](#)[References](#)[Tables](#)[Figures](#)[◀](#)[▶](#)[◀](#)[▶](#)[Back](#)[Close](#)[Full Screen / Esc](#)[Printer-friendly Version](#)[Interactive Discussion](#)

The Arctic low ozone period 2011

R. Hommel et al.

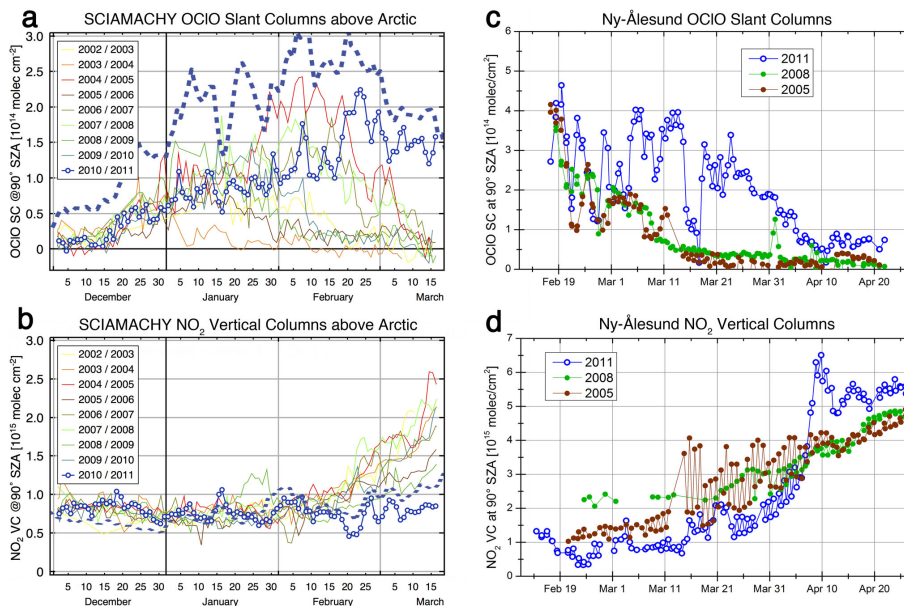


Fig. 10. SCIAMACHY observations (**a** and **b**) and ground-based measurements of OCIO slant columns (**a** and **c**) and vertical columns of NO_2 (**b** and **d**) in the Northern Hemisphere since winter 2002/2003 at 90° SZA. Ground-based measurements in Ny-Ålesund (79°N , 12°E) were carried out in winter–spring 2005, 2008, and 2011. CTM calculations for winter–spring 2010–2011 are shown as a dashed line in SCIAMACHY plots and were sampled at 90° SZA at the time of SCIAMACHY overpass.

Title Page

Abstract

Introduction

Conclusions

References

Tables

Figures

◀

▶

◀

▶

Back

Close

Full Screen / Esc

Printer-friendly Version

Interactive Discussion



The Arctic low ozone period 2011

R. Hommel et al.

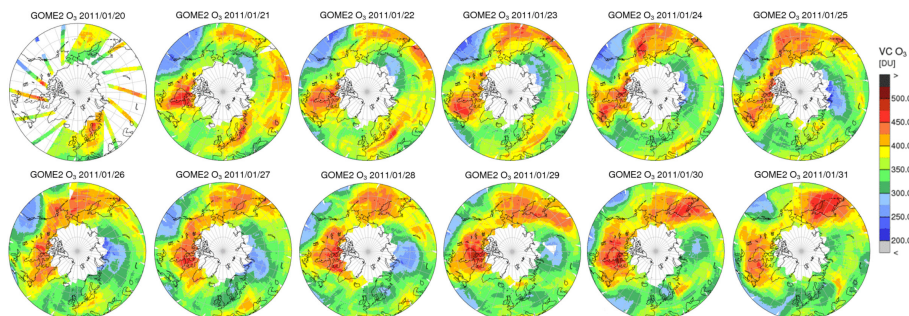


Fig. 11. Daily maps of total ozone measured by GOME-2 between 20 and 31 January 2011. On 21 January 2011 column ozone was substantially lowered by more than 70 DU over Central Siberia north of Sakhalin, and was moving westwards to the Ural region. After 28 January 2011 the area of low ozone moves eastward and dissolves at approximately 90–100° E/60° N on 30 January.

[Title Page](#)[Abstract](#)[Introduction](#)[Conclusions](#)[References](#)[Tables](#)[Figures](#)[◀](#)[▶](#)[◀](#)[▶](#)[Back](#)[Close](#)[Full Screen / Esc](#)[Printer-friendly Version](#)[Interactive Discussion](#)

The Arctic low ozone period 2011

R. Hommel et al.

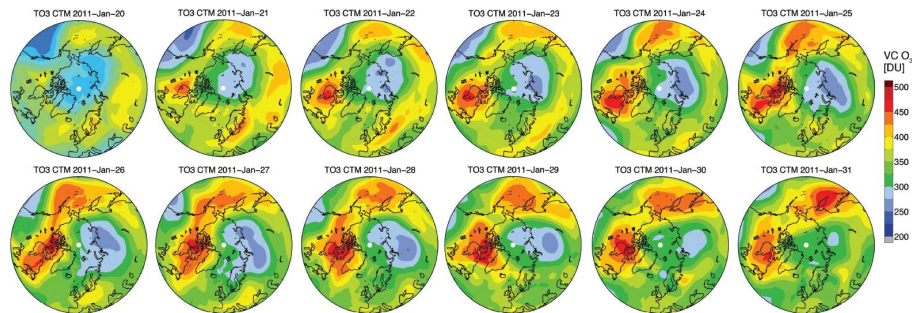


Fig. 12. As in Fig. 11, except for model total ozone. In contrast to Fig. 4, here the Fortuin and Kelder (1998) climatology of tropospheric ozone was added to the model's stratospheric ozone column in order to cover the entire atmosphere.

[Title Page](#)[Abstract](#)[Introduction](#)[Conclusions](#)[References](#)[Tables](#)[Figures](#)[◀](#)[▶](#)[◀](#)[▶](#)[Back](#)[Close](#)[Full Screen / Esc](#)[Printer-friendly Version](#)[Interactive Discussion](#)

The Arctic low ozone period 2011

R. Hommel et al.

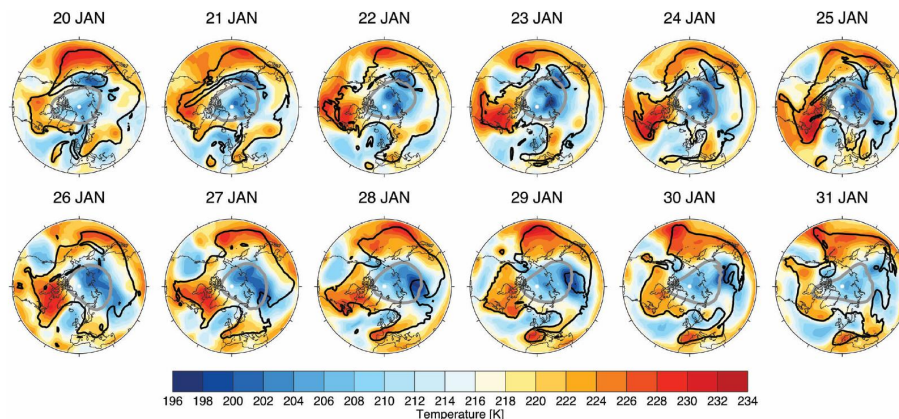


Fig. 13. Twelve day sequence of temperature at approximate tropopause level (315 K isentropic surface) during the period when large reductions in the GOME-2 column ozone are observed (Fig. 11). The vortex edge is indicated by the grey contour of the 38 PVU potential vorticity at the 475 K isentropic. The thick black contour denotes the 3 PVU potential vorticity at 315 K, roughly separating polar air masses (low tropopause) from subtropical air masses (high tropopause). All data were obtained from the ECMWF ERA-Interim reanalysis.

[Title Page](#)[Abstract](#)[Introduction](#)[Conclusions](#)[References](#)[Tables](#)[Figures](#)[◀](#)[▶](#)[◀](#)[▶](#)[Back](#)[Close](#)[Full Screen / Esc](#)[Printer-friendly Version](#)[Interactive Discussion](#)

The Arctic low ozone period 2011

R. Hommel et al.

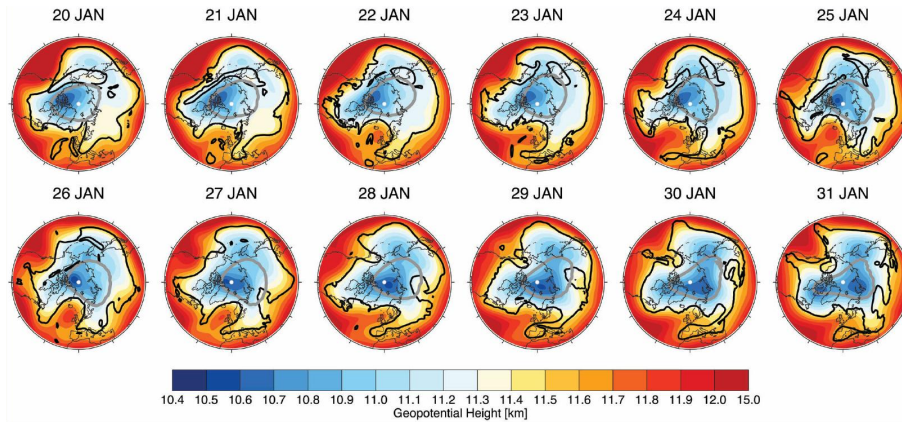


Fig. 14. As in Fig. 13 except for geopotential height.

Title Page

Abstract Introduction

Conclusions References

Tables Figures

◀ ▶

◀ ▶

Back Close

Full Screen / Esc

Printer-friendly Version

Interactive Discussion



The Arctic low ozone period 2011

R. Hommel et al.

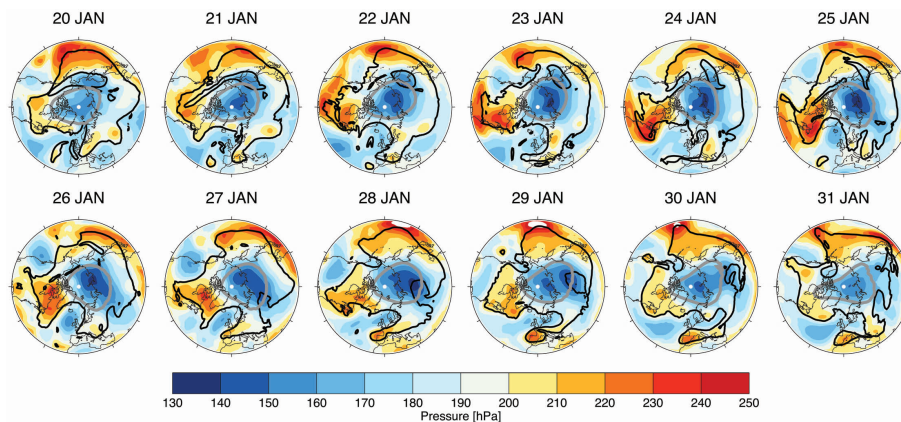


Fig. 15. As in Fig. 13 except for pressure at the 350 K isentropic surface.

[Title Page](#)[Abstract](#)[Introduction](#)[Conclusions](#)[References](#)[Tables](#)[Figures](#)[◀](#)[▶](#)[◀](#)[▶](#)[Back](#)[Close](#)[Full Screen / Esc](#)[Printer-friendly Version](#)[Interactive Discussion](#)